Ecological Informatics 92 (2025) 103501

Contents lists available at ScienceDirect

Ecological Informatics

journal homepage: www.elsevier.com/locate/ecolinf

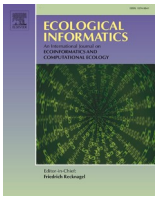

Characterizing pelagic pair trawl partnerships using coordination metrics and behavior classification in the Black Sea

Taner Yıldız [a,1,*], Alessandro Galdelli [b,c,1,**], Nurdan Cömert [a], Adriano Mancini [b], Anna Nora Tassetti [c,d]

[a] Department of Fisheries Technology and Management, Faculty of Aquatic Sciences, Istanbul University, Istanbul, Türkiye
[b] Department of Information Engineering, Università Politecnica delle Marche, Ancona, Italy
[c] National Biodiversity Future Center, Palermo, Italy
[d] National Research Council (CNR), Institute for Biological Resources and Marine Biotechnologies (IRBIM), Ancona, Italy

ARTICLE INFO

Keywords:
Pelagic trawl
AIS
Dyadic coordination
Clustering
Vessel classification
Black Sea

ABSTRACT

Pelagic pair trawling involves two vessels towing a single midwater net in coordinated motion to target schooling pelagic species. Monitoring and distinguishing pair-trawl operations remain challenging for fisheries management, particularly when analyses rely on single-vessel data. Focusing on the Turkish Black Sea, this study presents an AIS-based framework to identify and characterize cooperative behavior in pelagic pair trawling fleets. We combine Gaussian Mixture Models for speed-profile classification with dyadic coordination metrics based on spatial proximity, heading alignment, and speed synchronization. The results indicate a network of 70 vessels and 51 dyads that reveal a structured pattern of recurrent partnerships and transient collaborations, with short-term coordination events occurring at separations under 1 km and speed differences below 1 knot. Weekly networks revealed a pronounced winter-spring activity pulse, a shutdown during the national summer closure, and a post-ban resurgence in autumn. Cohesion peaked within compact subfleets structured around a few central hubs, while spatial footprints and port linkages indicated regional organization along the south-western and south-central coasts. Leader-follower scores clustered near parity, consistent with paired-gear constraints, and cross-recurrence of speed series showed high determinism and laminarity, reflecting stable, repetitive operational routines. By integrating behavioral, spatial, and temporal indicators, the framework enables objective detection of cooperative fishing and provides a transferable, data-driven approach to support monitoring, spatial management, and sustainable governance of cooperative pelagic trawl fleets.

1. Introduction

Marine fisheries in the Black Sea have undergone substantial transformations over recent decades, driven by technological advancements, increased fishing pressure, and evolving socioeconomic contexts (Akoğlu, 2023; Akoğlu et al., 2014). Advances in navigation, fish-finding technologies, and vessel power have reshaped where and how fishers operate, while changing market demands and regulatory frameworks have influenced which species are targeted. Collectively, these shifts have progressively modernized the regional fleet, fostering the diversification of fishing practices and strategies. As a result, a variety of fishing methods such as purse seining, bottom trawling, gillnetting, and pelagic trawling are now employed. Pelagic trawling differs from bottom trawling in that the nets are towed through midwater column rather than along the seabed, targeting schooling fish that inhabit open-water layers. When performed by two vessels working cooperatively to tow a net at midwater depths and target dense fish aggregations (Zengin et al., 2003), the method is known as pelagic pair trawling. This technique has emerged as a major fishing practice, due to its operational efficiency in capturing dense fishing aggregations of commercially important pelagic species such as sprat (*Sprattus sprattus*), anchovy (*Engraulis encrasicolus*), horse mackerel (*Trachurus trachurus*), and bluefish (*Pomatomus saltatrix*) (Dağtekin et al., 2021; Erdem and Özdemir, 2008). Furthermore, technological innovations in fish detection and gear operation using echo

* Corresponding author.
** Corresponding author at: Department of Information Engineering, Università Politecnica delle Marche, Ancona, Italy.
E-mail addresses: yldztnr@istanbul.edu.tr (T. Yıldız), a.galdelli@staff.univpm.it (A. Galdelli).
[1] Corresponding authors contributed equally.

https://doi.org/10.1016/j.ecoinf.2025.103501
Received 4 August 2025; Received in revised form 27 October 2025; Accepted 28 October 2025
Available online 30 October 2025

sounders and net sounders have improved the precision and efficiency of pelagic trawl fisheries (Zengin et al., 2003), thereby enhancing catch rates and economic viability of each fishing trip.

The widespread adoption of pelagic pair trawling is also driven by its distinct operational advantages. By eliminating the need for trawl doors, pair trawling reduces gear drag and associated fuel consumption. Comparative studies have demonstrated substantial benefits over solo trawling operations, including fuel savings of up to 40 % and catch increase of around 29 %, resulting from larger swept areas and enhanced fish-herding efficiency (McHugh et al., 2022). Consequently, reduced fuel consumption also lowers greenhouse gas emissions, contributing to both economic and environmental sustainability goals (Oliver et al., 2023). These advantages have encouraged the method's spread across regions, as fishing fleets gradually adapted it to local conditions and target species.

In the Black Sea, particularly in Turkish waters, pelagic trawl fishing gained momentum in the late 20th century, becoming economically preferable to traditional bottom trawling due to its higher profitability and reduced impact on benthic habitats (Dağtekin et al., 2021).

The Black Sea is characterized by strong stratification, limited water exchange with the Mediterranean, and high nutrient inflows from major rivers such as the Danube, Dniester, and Dnieper. These conditions support productive coastal shelves and abundant pelagic fish assemblages dominated by anchovy, sprat, and horse mackerel, providing ideal grounds for pelagic trawl fisheries. Pelagic pair trawling was first introduced to Türkiye from Italy in 1978, where it was already well established. Initially, it was used to target smooth-hound sharks (*Mustellus* spp.), but unexpected high winter catches of anchovy near the seabed soon prompted local fishers to adopt this technique more widely. Over time, modifications were made to adapt the Italian midwater trawl design to local conditions, including enlarging the mesh size in the forward sections and reducing it toward the cod end to better target small pelagic fish such as anchovies, sprats and horse mackerel (Erdem and Özdemir, 2008). The resulting gear, typically made of polyamide (nylon) with symmetrical panels, remains structurally similar but less technologically advanced than modern European designs (Ayaz et al., 2000). Technological components such as sonar, net-sounders, and echo-sounders are commonly used on Turkish vessels but are generally less advanced than those employed by contemporary European fleets, indicating opportunities for modernization and efficiency improvements (Gümüş and Zengin, 2011). Pelagic pair trawling gained particular prominence in the Yeşilırmak-Kızılırmak shelf during the 1990s and became widespread by the early 2000s, when around 40 vessel pairs were active in the region (a number that has since increased to approximately 60–70 pairs). Midwater trawling targeting bluefish is particularly common along the Western Black Sea coast, between Şile and Karadeniz Ereğlisi (Knudsen and Zengin, 2006).

At present, pair pelagic trawling in the Black Sea is practiced exclusively by Türkiye, whereas Bulgaria employs single-vessel pelagic trawling operations. Türkiye's pelagic trawl fishery primarily targets sprat, anchovy, and horse mackerel, with catches strongly influenced by environmental conditions, fish schooling behavior, and operational parameters such as vessel speed, trawl design, and timing of fishing activities (Erdem and Özdemir, 2008; Samsun et al., 2006). In Türkiye, midwater trawling is legally permitted but regulated through seasonal and spatial restrictions, with vessels licensed specifically for pelagic pair trawling. However, administrative records and public registries do not systematically indicate which vessels operate together as pairs at any given time. Furthermore, vessels are allowed to change their declared primary gear type once per year, yet whether they fish using the newly declared gear cannot be verified from registry data alone. These institutional limitations highlight the need to infer pelagic pair trawling behavior directly from vessel movement data rather than relying solely on static registry labels.

Although pelagic trawling is economically important, concerns regarding sustainability and fisheries management persist. Factors such as overfishing, fleet overcapacity, climate change, and ecosystem changes continue to threaten fish stocks and fisheries' sustainability (Dağtekin et al., 2021). The high operational efficiency and associated fishing pressure of pair trawling raise ecological and management challenges, especially due to its potential effects on fish school structures. Potential mechanisms include dual vessel herding that compacts or fragments schools, repeated towing through aggregations that alters cohesion, and localized depletion that alters school size distribution and spatial organization, ultimately increasing fishing mortality (Joo et al., 2018; Joo et al., 2021). In this context, identifying which vessels form pelagic pairs, where and when they operate, and how their spatial footprints evolve provides actionable evidence for monitoring, enforcing seasonal and depth-based restrictions, and supporting gear-specific spatial planning for sustainable resource use. Moreover, recognizing paired operations also yields a more realistic estimate of fishing effort, as it avoids double-counting both vessels within a pair.

Considering the above, the identification and characterization of collective behaviors, such as those observed in pelagic pair trawling, have recently attracted significant scientific attention (Joo et al., 2015; Joo et al., 2018). To quantitatively assess these collective patterns, dyadic movement analyses, using metrics such as proximity, directional synchrony, and displacement similarity, provided a robust framework for detecting coordinated vessel behavior from spatial and temporal data (Joo et al., 2021). This research field has been propelled by the increasing availability of vessel's spatio-temporal tracking data from sources such as the Automatic Identification System (AIS; Brandoli et al., 2022; Coro et al., 2021; de Souza et al., 2016), Vessel Monitoring System (VMS; Hintzen et al., 2012; Hinz et al., 2013; Vermard et al., 2010) and Navigation Satellite Systems devices (GNSS; Mendo et al., 2023; Rufino et al., 2023; Samarão et al., 2025). These datasets proved valuable for mapping fishing activities and for gear-specific behavior inference when supported by transparent, reproducible methods (Hintzen et al., 2025); and have enabled a proliferation of descriptive mapping efforts (Ferrà et al., 2018; Yildiz et al., 2025) and studies characterizing fishers' spatial dynamics and behavioral classification (Galparsoro et al., 2024; Henriques et al., 2024; Letschert et al., 2025; Maina et al., 2018; Vermard et al., 2010; Watson and Haynie, 2016; Zhang et al., 2022). They also complement (and, where necessary, substitute for) incomplete or non-integrated logbook and registry information (Coro et al., 2022; Pulcinella et al., 2023), which typically lack the temporal resolution required to capture dynamic interactions.

In parallel, the growth of ecological informatics, machine learning has fostered new approaches to analyzing movement ecology (Rubbens et al., 2023), enabling researchers to transform such massive trajectory datasets and descriptive mapping into mechanistic understanding of spatial organization in marine fleet dynamics, interpretable models of coordination, interaction, and behavioral structure (Gillis et al., 2021; Liu et al., 2022; Yang et al., 2024).

Despite these advances, applying data-driven frameworks to specific regional fisheries is challenging, as differences in regulation, fleet composition, operational behavior, and data availability demand tailored analytical approaches. Addressing this challenge, the present study focuses on the Turkish pair pelagic trawl fleet in the Black Sea, where pair operations are widespread yet poorly documented, to demonstrate how AIS-based ecological informatics can reveal coordinated fishing behavior at scale. To this end, we propose an integrated analytical framework that leverages AIS-derived trajectories to quantify behavioral coupling and identify recurring coordination patterns at the fleet level by applying unsupervised learning (k-means clustering), graph-theoretical modeling, spatiotemporal dyadic metrics, and recurrence-based time series analysis. The combination of vessel classification, proximity-based interaction metrics, and network topology provided scalable and reproducible insights into cooperative fishing strategies, advancing toward the development of vessel association networks that capture the interconnections between human behavior, technology, and ecosystem processes in fishing activity (Gillis et al.,

2021).

While prior studies have mapped fishing effort or characterized vessel movements at coarse spatial resolutions, few have investigated fine-scale temporal coordination and behavioral coupling within operational fishing dyads. In particular, the dynamics of pair trawling remain largely underexplored. To our knowledge, this study represents one of the first applications of an ecological informatics approach to characterize cooperative fleet behavior in the Black Sea using AIS-derived dyadic networks, coordination metrics, and nonlinear movement analysis.

2. Materials and methods

This study employed high-resolution AIS data to investigate potential coordinated fishing activities in the Black Sea, among Turkish-flagged fishing vessels. The initial AIS dataset (sourced from the Astra Paging[2] provider) contained time-stamped positional records including Maritime Mobile Service Identity (MMSI), geographic coordinates (latitude and longitude), speed over ground (SOG), and navigational course. The resulting raw AIS dataset consisted of 4,970,928 rows and represented all vessels operating in the Black Sea during 2022 which is preprocessed. Each MMSI represents a unique numerical identifier assigned to the AIS transponder of a vessel, enabling individual trajectory reconstruction and linkage with the national vessel registry. SOG indicates a vessel's instantaneous velocity relative to the Earth's surface, while course-over-ground specifies its directional heading with respect to true north. These dynamic variables collectively provide the empirical basis for quantifying vessel movement and co-movement patterns. The systematic use of the data makes it possible to infer instances of coordinated navigation corresponding to cooperative trawling behavior analyzing how vessels with distinct MMSI identifiers converge spatially and maintain similar SOG and course values over time. Fig. 1 provides a summary of the analytical framework and all the involved processing steps.

2.1. Administrative registry data

A complementary static reference dataset was necessary to contextualize the information extracted from AIS trajectories within the administrative structure of the Turkish fleet. We obtained the official 2022 national fishing-vessel registry from the Republic of Türkiye Ministry of Agriculture and Forestry through a formal request. The registry enumerates 448 licensed fishing vessels, of which 64 hold explicit authorization for pelagic pair trawling. However, we observed that this list was different from the General Fisheries Commission for the Mediterranean (GFCM) list therefore we started a conservation with a fisher society and found 16 vessels started season with pelagic trawl and then shifted their fishing gear to bottom trawl. We determined that a total of 80 vessels, for which the dataset includes the following fields: Vessel Name, Fleet Registration Number, License Code Number, MMSI number, Vessel Length, and Gear Type. We used this registry to (i) define the a priori population of vessels considered in our analyses and (ii) reconcile AIS-based gear labels with administrative designations. The registry does not contain operational logbook information or day-to-day pairing records. Together, the AIS and registry datasets formed the foundation for all subsequent preprocessing and analytical steps described below.

2.2. AIS data preprocessing

AIS records were preprocessed to isolate fishing vessels in the region of interest and our analysis focused exclusively on Turkish vessels by filtering records whose CALLSIGN values began with the national prefix "TC". Furthermore, vessel positions reporting speeds greater than 20 knots were discarded, following the findings and suggestions of the study by Ferrà et al. (2020). This upper threshold was chosen to exclude implausible measurements, caused by transmission and sometimes due to sensor errors, and to remove high-speed vessels such as passenger ferries, naval craft, or other non-fishing entities that fall outside the scope of this study.

We developed and evaluated two distinct AIS data processing pipelines to identify coordinated fishing behavior. The first, a trip-based approach, segmented vessel trajectories into discrete fishing trips based on proximity to known port locations and temporal continuity thresholds. While this method facilitated behavioral interpretation on a trip level, it exhibited limited robustness in the presence of AIS transmission gaps or asynchronous port detection. The second approach implemented a timestamp-based dyadic matching algorithm, which evaluated vessel pairings at each AIS transmission independently of trip boundaries. This multistep pipeline allowed for fine-grained spatiotemporal comparisons of vessel proximity, course alignment, and speed similarity without relying on complete trip records. After a structured comparative assessment, we adopted the timestamp-based approach as the primary analysis path. This method was better suited to the geographical operational characteristics of the Turkish pelagic trawling fleet in its intermittent AIS behavior and potential gear-switching dynamics. Moreover, the timestamp-based approach yielded higher dyadic coverage and improved identification rates for known pelagic pair trawlers.

2.3. Port proximity filtering

AIS points that likely corresponded to port entry, exit, or idling near harbors were further removed to minimize noise from non-fishing operations. A list of known Turkish fishing ports with verified geographic coordinates was used as a reference. A spatial buffer of 1 km was applied around each port coordinate, and AIS points located within this buffer zone were flagged and excluded. Distances were calculated using the Haversine formula via the distHaversine() function from the `geosphere` R package (Hijmans, 2024), which accounts for the curvature of the Earth when computing great-circle distances. Only records that were farther than 1 km from all listed ports were retained.

2.4. Conversion to spatial object and geometry management

Spatial consistency was ensured by converting the filtered dataset into an sf object using the st_as_sf() function from the *sf* R package (Pebesma and Bivand, 2023). This conversion allowed direct manipulation of georeferenced data within the WGS 84 coordinate reference system (EPSG:4326), maintaining geospatial accuracy throughout the workflow. For operations requiring a purely tabular structure, such as many-to-many joins and time-series comparisons, a non-spatial version of the dataset was generated using the st_drop_geometry() function.

2.5. Construction of vessel dyads and temporal matching

Candidate vessel pairs exhibiting spatiotemporal proximity were identified by constructing dyads for each timestamp containing multiple recorded vessels. At each timepoint, all possible two-vessel combinations were generated using the combn() function, and the resulting dyads were expanded into individual rows annotated with the corresponding MMSI identifiers. Two sequential left_join() operations were then performed to enrich each dyad with the associated positional and navigational attributes (latitude, longitude, speed, and course) of both vessels, derived from the non-spatial AIS dataset. This procedure ensured precise temporal alignment of location and movement features for every vessel pair within each observation interval.

[2] www.astrapaging.com

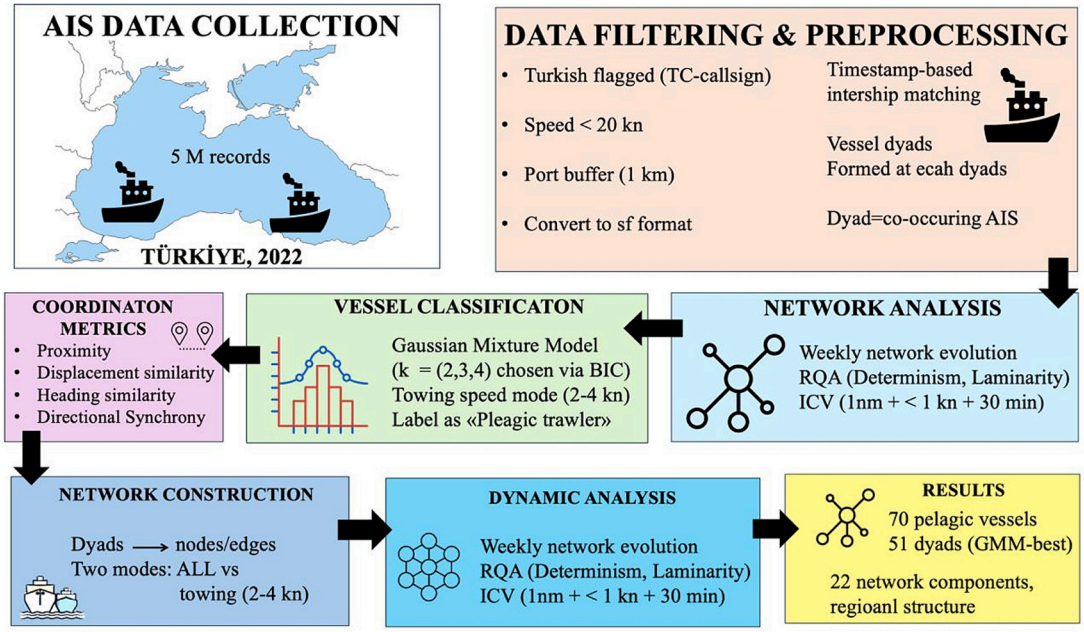

Fig. 1. Overview of the analytical pipeline to detect and characterize pelagic pair trawling partnerships in the Turkish Black Sea. AIS data were filtered, dyadic coordination metrics computed, and vessel types classified via Gaussian mixture modeling. Networks of candidate dyads were constructed and analyzed dynamically, incorporating recurrence-based time series metrics and intermittent coordination windows.

2.6. Calculation of interaction metrics

The level of coordinated behavior between vessels was quantified through four distinct interaction metrics: proximity index, heading similarity, displacement similarity, and directional synchrony. The formulas follow the methodology presented by Joo et al. (2021). Consider two vessels i and j and observed concurrently at discrete UTC timestamps $\tau = 1, \ldots, T$. Each vessel's position is denoted as $x_i(\tau) = (\mathrm{lon}_i(\tau), \mathrm{lat}_i(\tau))$ in the WGS84 coordinate system, with course-over-ground $\theta_i(\tau) \in [0^\circ, 360^\circ)$ expressed in degrees, and speed-over-ground $v_i(\tau) \geq 0$ measured in knots (kn). Great-circle distances between vessels were computed using a Haversine or ellipsoidal formulation, expressed in meters.

The dyadic observation set is defined as $W_{ij} = \{\tau : \text{both } i, j \text{ observed at } \tau\}$, and, for lag-based quantities, as $W_{ij}^{-} = \{\tau \in W_{ij} : \tau - 1 \in W_{ij}\}$, representing time steps where both vessels are concurrently observed at consecutive timestamps. In the towing-restricted configuration, W_{ij}^{-} was further constrained to times when both vessels were classified as "towing" at τ.

- *Proximity Index*: The proportion of time during which the two vessels were within 1000 m of each other, computed using the Haversine distance. This metric captures physical nearness over time. For a distance threshold $d_0 = 1000$ m and an infinitesimal ε to avoid division by zero (Long et al., 2014),

$$d_{ij}(\tau) = dist\big(x_i(\tau), x_j(\tau)\big), Proximity_{ij} = \frac{1}{|W_{ij}|}\sum_{\tau \epsilon W_{ij}} 1\{d_{ij}(\tau) \leq d_0\}$$

- *Heading Similarity (DI_h)*: Heading similarity (DI_h) was computed as the mean cosine of the wrapped heading difference across shared timestamps (Long et al., 2014); wrapped on $(-\pi,\pi]$ following standard circular statistics (Fisher, 1993; Mardia and Jupp, 1999). Higher values suggest more aligned navigation paths. Let W_{ij} be the set of timestamps at which vessels i and j are both observed. Let $\theta_i(t)$, $\theta_j(t) \in [0,2\pi)$ denote their course-over-ground (in radians) at time $t \in W_{ij}$. Define the wrapped angular difference

$$\Delta\theta_{ij}(t) = wrap_{(-\pi,\pi]}\big(\theta_i(t) - \theta_j(t)\big),$$

which maps any angle to $(-\pi, \pi]$. The heading similarity between i and j is

$$DI_h(i,j) = \frac{1}{|W_{ij}|}\sum_{t \epsilon W_{ij}} \cos\big(\Delta\theta_{ij}(t)\big), \epsilon[-1,1].$$

- *Displacement Similarity (DI_d)*: For each vessel, stepwise displacements between consecutive AIS points were computed using geodesic distances. DI_d represents the average normalized difference in these displacements, adjusted by their speed differences. The metric evaluates how similar these stepwise displacements are between two vessels observed simultaneously. To achieve this, we first define the one-step displacement for each vessel as the distance between its consecutive positions, then compute a normalized contrast representing the relative difference between the two vessels' displacements. A similar normalization is applied to instantaneous speed differences, ensuring that the comparison remains scale-invariant with respect to absolute vessel speed. These per-step similarity scores are subsequently aggregated over the entire observation period to obtain the overall displacement similarity index DI_d, which captures how consistently the two vessels move in synchrony across time. The one-step displacements for each vessel and a normalized contrast are defined as follows:

$$\Delta s_i(\tau) = dist(x_i(\tau), x_i(\tau - 1)), \delta_s(\tau) = \frac{|\Delta s_i(\tau) - \Delta s_j(\tau)|}{\Delta s_i(\tau) + \Delta s_j(\tau) + \varepsilon} \in [0,1].$$

Similarly, define a normalized instantaneous speed difference

$$\delta_v(\tau) = \frac{|v_i(\tau) - v_j(\tau)|}{v_i(\tau) + v_j(\tau) + \varepsilon} \in [0,1).$$

We then compute a per-step similarity score

$$c(\tau) = 1 - \delta_s(\tau)[1 - \delta_v(\tau)] \in [0,1],$$

and aggregate

$$DI_{d,ij} = \frac{1}{\left|W_{ij}^{-}\right|} \sum_{\tau \in W_{ij}^{-}} c(\tau).$$

- *Direional Synchrony (DI_{θ})*: Directional synchrony was computed as the mean cosine of the wrapped heading difference across all shared timestamps, following dynamic-interaction formulations (Long et al., 2014) and circular-statistics conventions for angle wrapping (Fisher, 1993; Mardia and Jupp, 1999). A directional alignment metric computed as the average cosine similarity of headings across the full dyad time series, independent of instantaneous proximity. Using circular difference and cosine similarity,

$$\Delta\theta_{ij}(\tau) = \theta_i(\tau) - \theta_j(\tau), DI_{\theta,ij} = \frac{1}{\left|W_{ij}^{-}\right|} \sum_{\tau \in W_{ij}^{-}} \cos\left(\frac{\pi}{180} \Delta\theta_{ij}(\tau)\right).$$

All metrics were aggregated over the observation period for each unique dyad. Dyads with missing values in any metric were excluded to ensure robustness.

2.7. Filtering candidate dyads exhibiting coordinated behavior

Candidate dyads indicative of coordinated or pair trawling behavior were identified by applying joint thresholds across four spatiotemporal coordination metrics. Only vessel pairs that simultaneously satisfied all the following conditions were retained:

- Proximity >0.5
- Directional heading synchrony (DI_h) > 0.5
- Displacement similarity (DI_d) > 0.5
- Directional synchrony (DI_θ) > 0.5

These conditions select pairs that remain close in space, maintain coherent headings, and show synchronized movement that are hallmarks of pair trawling. The choice of 0.5 as a base cutoff follows methodological precedent in vessel-behavior studies (Joo et al., 2018) that use ≥0.5 to distinguish intentional coordination from incidental co-location. The theoretical range of the coordination metrics, as defined in the dyadic movement literature (Joo et al., 2018), is as follows: Proximity ∈ [0,1]; Displacement similarity (DI_d) ∈ [0,1]; and directional metrics (DI_h and DI_θ) ∈ [−1,1], reflecting their cosine- and threshold-based constructions.

Applicability to Black Sea fisheries was assessed through a sensitivity analysis in which each coordination threshold was independently varied over the range 0.40–0.60 (Δ = 0.05), while the remaining parameters were held constant at 0.5. For each configuration, the interaction network was recomputed, and deviations from the baseline (all four thresholds set to 0.5) were quantified using four complementary network-level metrics: edge-set Jaccard similarity (Jaccard, 1901, 1908), network density (Newman, 2010; Wasserman and Faust, 1994), giant-component fraction (Barabási, 2016; Newman, 2010), and degree-rank Spearman correlation (Spearman, 1904). All computations were implemented using the *igraph* package (Csardi and Nepusz, 2006).

2.8. Edge-set Jaccard similarity (vs baseline)

Quantifies the overlap between the set of dyadic edges identified at a given threshold and the baseline configuration, where all four cutoffs are fixed at 0.5.

$$J(E_\theta, E_0) = \frac{|E_\theta \cap E_0|}{|E_\theta \cup E_0|} \in [0,1].$$

2.9. Network density

For an undirected simple graph G = (V, E), the density is defined as

$$\text{density}(G) = \frac{2|E|}{|V|(|V|-1)}.$$

This metric was computed using the *edge_density* function in *igraph*.

2.10. Giant-component fraction

Let C_{max} be the largest connected component.

$$\text{giant\_frac}(G) = \frac{|C_{\max}|}{|V|}.$$

Connected components were identified using *igraph* utilities, and the fraction was obtained as the ratio between the size of the largest component and the total number of nodes.

2.11. Degree-rank Spearman correlation (vs. baseline)

Measures the rank correlation between node degrees in the perturbed network G_θ and the baseline network G_0, computed over the union of nodes. Nodes absent from one graph were assigned a degree of zero. Spearman correlations were computed using degree vectors, while cases in which one vector was constant (for example, an empty graph) were reported as *Not Applicable (NA)*.

For each configuration, the resulting interaction network was compared with the baseline graph (all thresholds set to 0.50), which contained 201 nodes, 2269 edges, a density of 0.1129, 44 components, and a giant-component fraction of 0.214. Variations in DI_h and DI_θ had negligible effects on network structure, with edge counts ranging from 2175 to 2269 (median Jaccard similarity = 1.000, minimum = 0.924) and median degree-rank Spearman correlation ρ = 1.000. The DI_d metric exhibited a similarly stable behavior (edges 2262-2271; median Jaccard = 0.994, range 0.983–1.000; median ρ = 0.9997), indicating that directional and displacement similarity thresholds around 0.50 do not materially affect network topology.

In contrast, sweeping the Proximity threshold produced more pronounced structural changes, with edge counts varying from 1824 to 2764 (median 2269) and a median density of approximately 0.116. Similarity to the baseline remained high (median Jaccard = 0.851, range 0.570–1.000) and the degree correlation maintained a median ρ = 0.814. Node retention remained 100 % for thresholds ≤0.50 but declined to 75.6 % at 0.55 and 70.6 % at 0.60, explaining the apparent increase in density at higher thresholds as the network contracts into a smaller, more cohesive core. Edge turnover relative to the baseline was modest at lower thresholds (+30 at 0.40; +4 at 0.45), while higher thresholds pruned weaker connections (−67 at 0.55; −74 at 0.60). A core-edge analysis revealed 202 edges persisting in at least 80 % of proximity settings, all of which were retained at 0.50 (Figs. 2 and 3).

Overall, these diagnostics demonstrate that (i) DI-based metrics are robust to reasonable threshold variation, and (ii) a proximity threshold of 0.50 provides an optimal balance by preserving the stable backbone of collaborative ties while minimizing incidental co-locations. Increasing the threshold above 0.55 eliminates substantial network content without qualitative improvement, whereas lowering it primarily introduces weak, non-core connections. Consequently, a value of 0.50 was retained as the primary threshold for all four coordination metrics, and complete sensitivity curves are reported for reference.

2.12. Vessel type classification based on speed profiles

The speed-profile classifier was calibrated using a reference set of vessels known to operate pelagic pair trawls (n = 45 MMSIs). From the AIS archive, only records associated with Turkish callsigns ("TC") and speeds ≤20 kn were retained. For each vessel, a speed vector was constructed, non-finite values were removed, and speeds were truncated to the range [0.25, 25] kn. When necessary, data were randomly down-

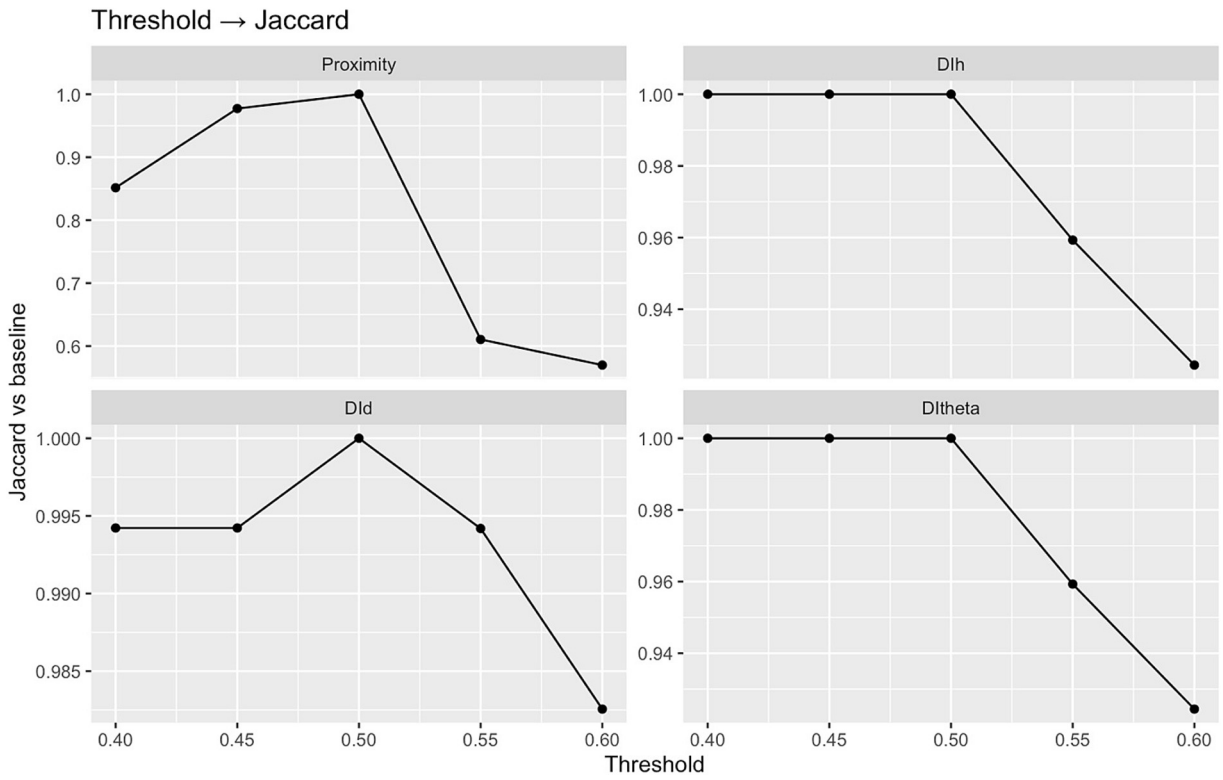

Fig. 2. Sensitivity of the inferred dyad set to the choice of interaction threshold. For each metric (facets: Proximity, DI_h, DI_d, DI_θ), the y-axis shows the Jaccard similarity between the edge set obtained at a given threshold (x-axis) and the baseline network used in the main analysis (GMM-BEST thresholds).

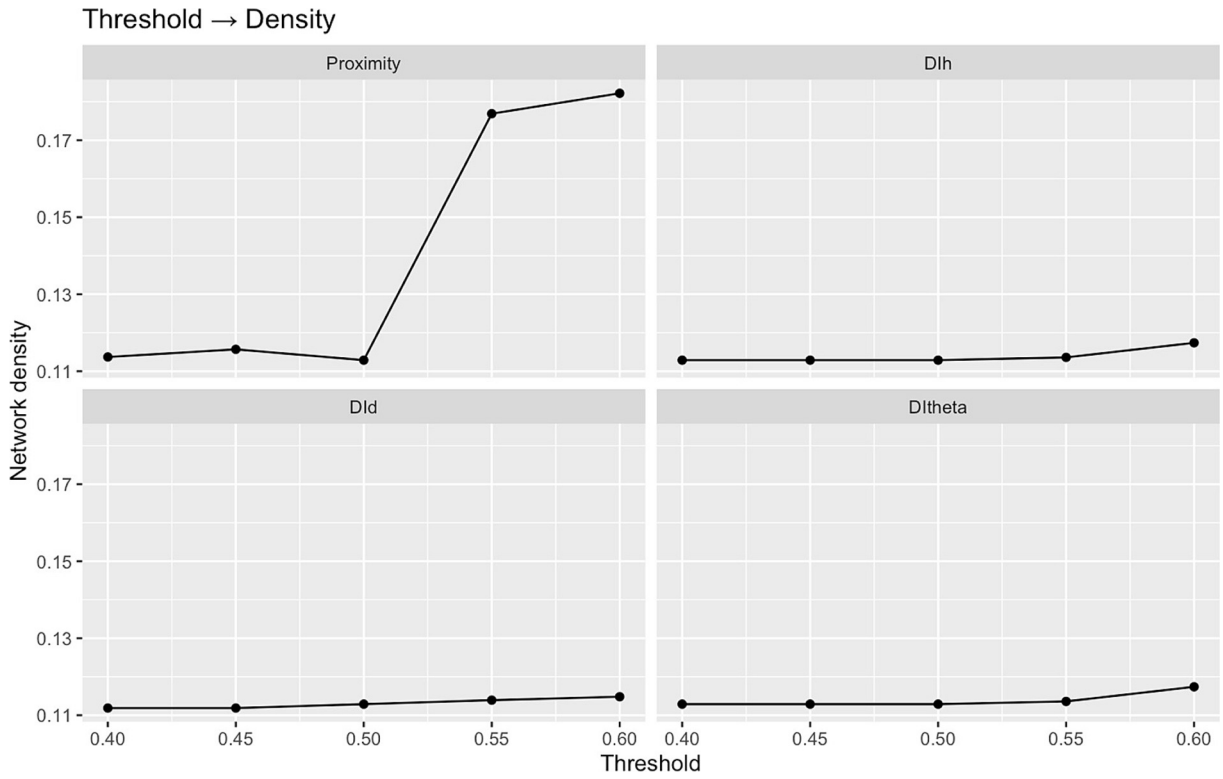

Fig. 3. Effect of interaction thresholds on overall network density. Each panel shows the density of the network reconstructed at the indicated threshold (x-axis) for a single metric while other filters follow the baseline settings.

sampled to a maximum of 2000 observations per vessel to control runtime. Vessels with fewer than 100 valid speed observations or lacking a detectable activity signal, defined as at least ten pings within either the towing (2–4 kn) or steaming (6–10 kn) ranges, were excluded. These two speed bands correspond to the operational modes of pelagic trawlers, as supported by previous AIS-based fisheries studies (Cheng et al., 2025; de Souza et al., 2016; Natale et al., 2015; Poos et al., 2020) and confirmed through calibration with a reference set of verified trawling vessels by field experts. Each vessel's speed distribution was modelled using univariate Gaussian mixtures with $k \in \{2, 3, 4\}$. The primary fitting routine employed the *mclust::Mclust* function (models "E" and "V"), with model selection based on the Bayesian Information Criterion (BIC; larger values indicating better fit). If *mclust* failed to converge, the model was refit using mixtools::normalmixEM, where BIC was computed under the conventional definition (smaller = better). To ensure comparability across libraries, a unified selection score was defined as BIC for mclust and -BIC for mixtools, with the model maximizing this score retained. Model-selection strength was evaluated using ΔBIC (difference between the best and second-best models), categorized following Kass and Raftery's guidelines ($\Delta < 2$: weak; 2–6: positive; 6–10: strong; >10: very strong).

From the selected Gaussian mixture, the towing component was identified as the mode with mean μ within 2–4 kn or, if absent, the mean closest to 3 kn (denoted $\mu_{t_o}w$). For diagnostic purposes, we also computed, for each k, the towing share (fraction of points assigned to the towing component under maximum a posteriori labeling) and a pelagic presence flag, defined as the existence of at least one component with a mean in both the towing (2–4 kn) and steaming (6–10 kn) bands.

Model selection results strongly favored richer Gaussian mixtures, with $k = 4$ selected for 33 of 45 vessels (73 %), $k = 3$ for 8 vessels (18 %), and $k = 2$ for 4 vessels (9 %). Evidence strength based on ΔBIC was largely decisive: "very strong" support for $k = 4$ in 31 vessels, for $k = 3$ in 8 vessels, along with two "strong $k = 4$," two "strong $k = 2$," and two "very strong $k = 2$" cases (Fig. 4). The towing-component mean ($\mu_{t_o}w$) clustered tightly around 3 kn, with a median of 2.99 kn (IQR = 2.86–3.33; range = 0.0004–4.90). Models with $k = 2$ exhibited lower and more variable $\mu_{t_o}w$ values, consistent with partial mixing of non-towing behaviors. Diagnostic checks confirmed that the fitted mixtures consistently resolved both towing (2–4 kn) and steaming (6–10 kn) modes in 3 vessels under $k = 2$, 29 under $k = 3$, and 39 under $k = 4$. The median towing share decreased from 0.642 ($k = 2$) to 0.163 ($k = 3$) and 0.111 ($k = 4$), indicating that models with $k \geq 3$ successfully separated additional behavioral states (e.g., searching or drifting) that simpler two-component mixtures tended to absorb.

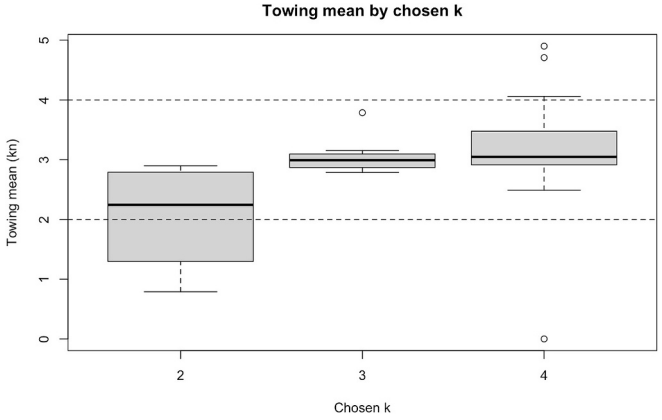

Fig. 4. Distribution of mean towing speeds (knots) for candidate pelagic pair trawling segments across different values of the chosen cluster parameter *k* (2, 3, and 4). Each box shows the median (thick horizontal line), interquartile range (box), whiskers (1.5 × IQR), and outliers (points). Horizontal dashed lines at 2 and 4 knots indicate the expected operational range for pelagic pair trawling, against which cluster solutions can be evaluated.

The speed distributions of pelagic pair trawlers exhibit clear multimodality, with four-component mixtures most frequently and most strongly supported (Fig. 4). The towing mode centered near 3 kn, as theoretically expected. These findings justify adopting mixtures with k ≥ 3, while retaining a $k = 4$ configuration for sensitivity analyses in subsequent fleet-wide classification.

For each MMSI in the candidate dyad pool, vessel type was classified solely based on its empirical speed distribution. Univariate Gaussian mixture models were fitted to the cleaned speed data, restricted to Turkish callsigns, speeds ≤20 kn, truncated to 0–25 kn, with a maximum of 2000 samples and at least 50 valid pings. Two classification schemes were implemented.

In the BEST scheme, models with $k \in \{2, 3, 4\}$ were fitted and the one with the optimal score was selected, using the *mclust* BIC (higher values indicating better fit) when available, or the *mixtools* BIC (lower values indicating better fit) mapped to a unified scale for cross-library comparison. The $k = 4$ (forced) scheme was motivated by prior calibration on confirmed pelagic pair trawlers, for which mixtures with $k = 4$ were most strongly supported.

From each selected mixture, a vessel was labeled *pelagic_trawl* if the component means included one mode within 2–4 kn (towing) and another within 6–10 kn (steaming), with at least 5 % of total pings in each band. Otherwise, the vessel was labeled as "other". Vessels failing quality control, such as those with too few or degenerate speed samples, were left unlabeled.

Final candidate dyads were retained only when both MMSIs were labeled *pelagic_trawl* under a given scheme, producing two sets: C_BEST and C_{K = 4}, which were used for robustness evaluation. For transparency, we report for each scheme the number of labeled vessels, retained dyadic edges, unique MMSIs, and the overlap between schemes, including Jaccard similarity on nodes and edges, and degree-rank Spearman correlation. The BEST scheme is adopted in the main analysis, while $k = 4$ (forced) is used as a sensitivity benchmark.

2.13. Identification of participating vessels

From the final filtered set of dyads, a unique list of MMSI identifiers was extracted to determine the number of individual vessels involved in potential pair trawling activity. This allowed for the quantification of both the number of candidate dyads and the subset of the fleet displaying behavioral traits consistent with collaborative fishing operations.

2.14. Analysis set and modes

All subsequent analyses were performed on the dataset *final_candidate_gmm_best*, which includes unordered vessel pairs that met two conditions: (a) both vessels satisfied the coordinated-movement thresholds, and (b) both were classified as pelagic pair trawlers by the GMM-BEST speed-profile classifier (model order selected by BIC over k ∈ {2, 3, 4}).

Two operational modes were considered:

- *ALL pings:* includes all concurrent AIS position reports for each dyad.
- *TOWING-only:* includes only the subset of records where both vessels were simultaneously traveling within the 2–4 kn speed range, corresponding to the standard towing band for pelagic pair trawling.

2.15. Construction of the vessel interaction network

We built two undirected graphs (ALL, TOWING) over the MMSIs present in *final_candidate_gmm_best*. Each node represents a vessel, and an edge between two nodes (i, j) indicates that the corresponding dyad satisfied the coordination thresholds during the study period. Networks were computed using the *igraph* package and visualized with *ggraph*. For

each network, we report the number of nodes (|V|), edges (|E|), average degree ($\bar{k}$) and density (δ) that can be defined as:

$$\bar{k} = \frac{2|E|}{|V|}$$

$$\delta = \frac{2|E|}{|V|(|V|-1)}.$$

Plots display absolute values, without ad-hoc scaling. Node size encodes degree, and layouts are generated with the Fruchterman-Reingold force-directed algorithm. MMSI labels were omitted to improve visual clarity.

The network edge set was defined using the dyadic thresholds validated in the sensitivity analysis (Proximity, DI_h, DI_d, and $DI_\theta = 0.50$), which balance false co-locations against missed coordinated pairs and demonstrated robustness in the range 0.40–0.60.

2.16. Temporal evolution of network structure (weekly)

To examine seasonality and the summer industrial fishing closure, we constructed weekly (starting with Monday) snapshots for both modes. For each week *t*, we recomputed the number of edges ($|E_t|$), mean degree ($\bar{k}$), and network density (δ_t) using consistent dyadic criteria. Weeks were defined with the *lubridate* function floor_date (unit = "week", week_start = 1).

2.17. Leader-follower coordination analysis

At each concurrent timestamp (τ), MMSI1 was designated as leading MMSI2 when three conditions were simultaneously satisfied.

(1) Spatial proximity: the great-circle distance between vessels was less than or equal to 500 m (d(p1(τ),p2(τ)) ≤500 m), computed using the distHaversine() function from the geosphere package.
(2) Heading alignment: the absolute difference in course-over-ground was within 10° (|Δϕ(τ)| ≤ 10°), following the tolerance adopted by Mardia and Jupp (1999).
(3) Geometric position: given MMSI1's forward unit vector $u(\tau) = (\cos\phi_1, \sin\phi_1)$, MMSI1 was considered to be ahead when the dot product $u(\tau)^\top (p_1(\tau) - p_2(\tau)) > 0$ (Katz et al., 2011). The Leader Score was defined as the proportion of shared timestamps at which MMSI1 led MMSI2. Scores were computed for both the *ALL* and *TOWING* modes using *data.table*, *dplyr*, and *geosphere*, with distributions visualized as histograms in *ggplot2*.

2.18. Component structure and spatial mapping

Connected components were identified for each mode using the *components()* function in *igraph*. Component sizes, representing groups of vessels with recurrent pairwise coordination, are presented as bar charts.

For each component, all associated AIS positions were merged, and a convex hull polygon was computed using *sf* (st_convex_hull). Areas were calculated after reprojection to an equal-area coordinate system CRS (EPSG:4326) and expressed in square kilometers (km^2). These polygons represent the spatial extent of coordinated operations rather than the actual trawled seabed. The port connectivity map was produced using *rnaturalearth* and *sf* to render coastlines and boundaries.

2.19. Recurrence Quantification Analysis of dyadic speed coupling

We applied Recurrence Quantification Analysis (RQA) to assess the temporal coupling between vessel speeds using the `crqa` R package (Coco et al., 2021; Coco and Dale, 2014). AIS speed data were aggregated into 10-min intervals for each vessel using *data.table* and *lubridate*, then aligned by exact bin timestamps through an inner join. Each series was subsequently standardized (mean = 0, sd = 1). Dyads with fewer than 100 overlapping bins were excluded to ensure statistical reliability.

For each dyad, we constructed delay-embedded vectors with embedding dimension $m = 2$ and delay $\tau = 1$ (Takens, 1981)

$$x_i = [z_1(i), z_1(i+1)], \quad y_j = [z_2(j), z_2(j+1)].$$

where z_1, z_2 are the per-vessel z-scores of speed. The cross-recurrence matrix is

$$R_{ij} = \Theta\left(r - \left\|x_i - y_j\right\|_2\right), \qquad r = 0.5,$$

with Θ(·) the Heaviside step function. Because all variables were standardized, the recurrence radius $r = 0.5$ corresponds to 0.5 standard deviations ("z-units") in $\mathbb{R}^2$ (Marwan et al., 2007; Webber Jr. and Zbilut, 1994). We adopted the following parameters: Theiler window *tw* = 0 (Theiler, 1986), minimum diagonal length min.diag.line = 2, and minimum vertical line min.vert.line = 2. From $R_{i,j}$, we computed the standard RQA metrics (Marwan et al., 2007; Webber Jr. and Zbilut, 1994):

- *Recurrence Rate (RR)*. The fraction of recurrent points in the cross-recurrence plot, reflecting the overall similarity between the two time series.

$$RR = \frac{1}{NM}\sum_{i=1}^{N}\sum_{j=1}^{M} R_{ij} \in [0,1].$$

Low RR indicates sparse recurrences (weak coupling), while high RR denotes frequent revisiting of similar joint states.

- *Determinism (DET)*. Fraction of recurrent points that belong to diagonal lines (length ≥ ℓ_{min}; here $\ell_{min} = 2$). Let $P(\ell)$ be the number of diagonal lines of length ℓ (i.e., sequences with $R_{i+k,j+k} = 0, \ldots, \ell$-1):

$$DET = \frac{\sum_{l=l_{min}}^{\infty} lP(l)}{\sum_{i,j} R_{ij}} \in [0,1].$$

High DET values indicate directionally persistent, predictable co-evolution (long diagonal structures) between vessel speeds.

- *Laminarity (LAM)*. Fraction of recurrent points in vertical lines (length ≥ v_{min} here $v_{min} = 2$). With $V_{(v)}$ the number of vertical lines of length v (runs with $R_{i+k,j} = 1$):

$$LAM = \frac{\sum_{v=v_{min}}^{\infty} vV(v)}{\sum_{i,j} R_{ij}} \in [0,1].$$

High LAM reflects periods of laminar or intermittent behavior, during which one vessel maintains a nearly constant speed relative to the other.

- *Entropy of diagonal lengths (ENTR)*. Shannon entropy of the diagonal-line length distribution:

$$ENTR = -\sum_{l=l_{min}}^{\infty} p(l)\log p(l), p(l) = \frac{P(l)}{\sum_{u=l_{min}}^{\infty} P(u)}$$

Higher ENTR values indicate more complex and diverse temporal dynamics, whereas lower values suggest greater regularity and stability in co-movement patterns.

2.20. Intermittent coordination windows (ICW)

Using the aligned 10-min series, a bin is "coordinated" if distance <1 nm (1852 m) and absolute speed difference < 1 kn (ITU-R, 2001). A

rolling window of 3 consecutive bins (approximately 30 min) is flagged as an ICW when all bins are coordinated. For each dyad we counted ICW windows N_{ij}^{win} over the year and report ICW hours as (Long et al., 2014)

$$\mathrm{ICW}_{ij} = N_{ij}^{win} \times \frac{3 \times 10}{60}.$$

The 1 nm / 1 kn thresholds provide a balance between tolerance to AIS measurement noise and sensitivity to genuine synchronized motion (Harati-Mokhtari et al., 2007), while the 30-min temporal window minimizes spurious coincidences and corresponds to typical trawling bouts observed in the field (Godø et al., 1990).

2.21. Experimental settings

The analyses were carried out in the R environment using a combination of specialized packages, including *data.table*, *dplyr*, *tidyr*, *lubridate*, *sf*, *geosphere*, *igraph*, *ggraph*, *ggplot2*, *crqa*, zoo (Zeileis and Grothendieck, 2005), and rnaturalearth. Distances were computed as great-circle measurements in meters, while vessel speeds were expressed in knots and headings in degrees. In the time-series visualizations, weekly time steps correspond to the starting date of each week (Monday). The seasonal industrial fishing ban, in effect from 15 April to 1 September, is represented in the weekly plots as a grey shaded area to highlight its temporal extent within the dataset.

Following the open science principles promoted by Huettmann and Arhonditsis (2023), all the resources necessary to reproduce and validate the results of this study have been made publicly accessible. Both the sample data and the R scripts are available in an open repository at https://github.com/vrai-group/Characterizing-pelagic-trawl-in-the-Black-Sea.

3. Results

The initial step involved quantifying the data volume and tracking its progressive contraction through the filtering pipeline, followed by a comparison with the official registry maintained by the Ministry. The raw dataset contained 4,970,928 AIS position reports from 1011 vessels recorded in 2022 (Stage S0). Restricting the analysis to the Türkiye domain, defined by TC callsigns, vessel speeds $\leq$20 kn, and the exclusion of port-buffer zones, resulted in 694,045 AIS messages from 708 vessels (Stage S0b).

From this subset, we constructed the dyadic co-occurrence universe (Stage S1), comprising 20,039 unordered vessel pairs generated by 500 vessels that appeared together at least once within the same timestamp. For each dyad, we calculated T, the number of shared timestamps (i.e., concurrent AIS pings). Across all S1 pairs, the median T was 41 (IQR 18–80; 10th–90th percentiles: 8–124). Applying the four coordination thresholds (Proximity, $\mathrm{DI_h}$, $\mathrm{DI_d}$, and $\mathrm{DI_\theta} \geq 0.5$) refined the dataset to 154 vessels forming 106 candidate dyads (Stage S2; median $T = 43$, IQR 19–95; $p_{10} = 6$, $p_{90} = 127$). Incorporating the pelagic-trawler speed-profile classification for both vessels in each pair yielded the final interaction networks. Using the GMM-BEST scheme, where the optimal mixture order $k \in \{2, 3, 4\}$ was selected via BIC, resulted in 70 vessels connected by 51 dyads (Stage S3a; median $T = 60$, IQR 24–103; $p_{10} = 12$, $p_{90} = 197$). The $k = 4$-forced variant produced a nearly identical structure with 67 vessels and 49 dyads (Stage S3b; median $T = 59$, IQR

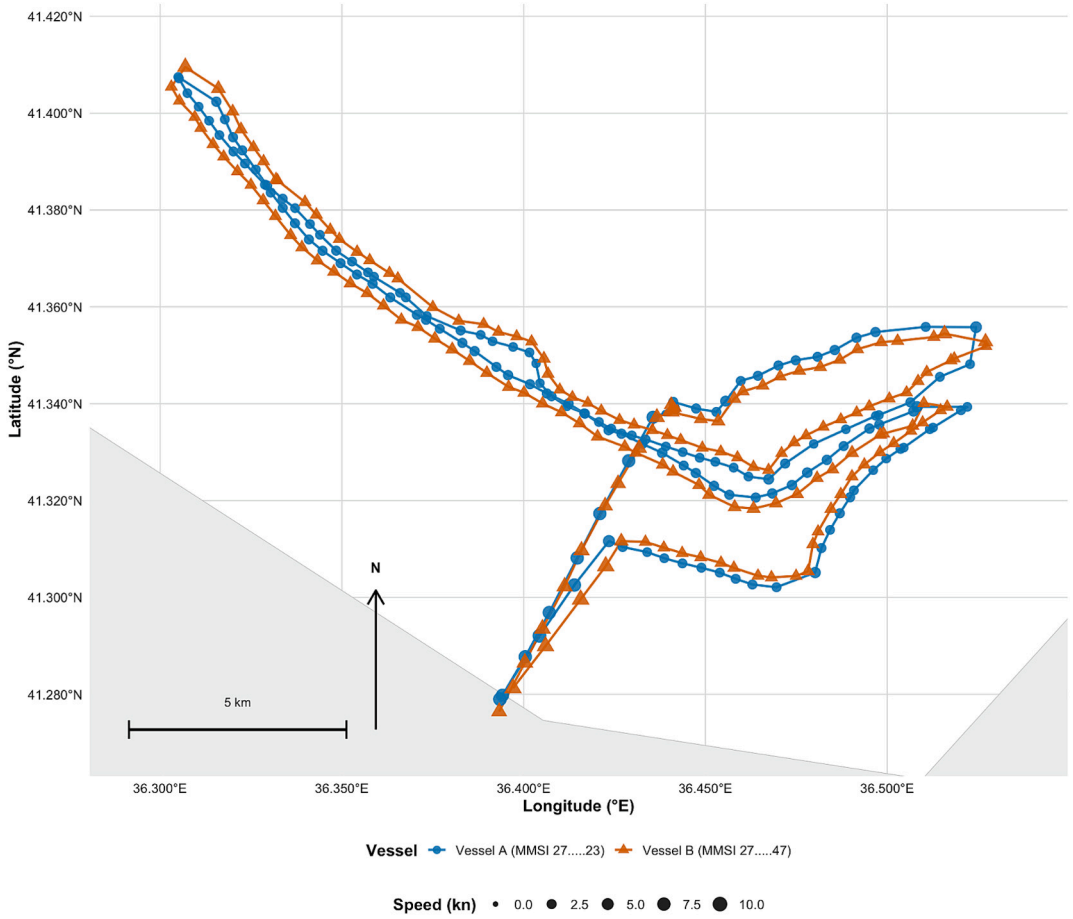

Fig. 5. AIS-derived movement trajectories of two Black Sea pelagic trawl vessels (MMSI 27…23 in orange and 27…47 in teal, respectively). Dot size encodes vessel speed (0–7 kn). The closely parallel tracks illustrate synchronized displacement behavior of the vessel pair. (For interpretation of the references to colour in this figure legend, the reader is referred to the web version of this article.)

27–103; $p_{10} = 14.9$, $p_{90} = 197$).

These results clarify that T represents the number of concurrent observations per dyad and tends to increase under stricter coordination and classification filters (median 60 in the final networks versus 41 in the unfiltered co-occurrence universe). An illustrative example is provided in Fig. 5, showing two pelagic trawlers (MMSI 27…23 and 27…47) exhibiting tightly parallel, speed-matched tracks. Point size encodes vessel speed (0−10kn), visually demonstrating the synchronized displacement patterns captured by our coordination metrics.

The evolution of the dataset through the filtering pipeline is summarized in Table 1, which reports, for each processing stage, the number of AIS position messages, unique vessels, and unordered vessel pairs (dyads) that co-occurred at least once (≥ 1 concurrent ping). For each stage, summary statistics of T (the number of shared timestamps per dyad) are provided, including the median, interquartile range (25th–75th percentiles), and 10th–90th percentiles. The final stages (S3a and S3b) correspond to dyads in which both vessels were classified as pelagic trawlers using Gaussian mixture models, either with model order selected by BIC (*GMM-BEST*, $k \in \{2, 3, 4\}$) or fixed at $k = 4$.

To benchmark these results, the final pelagic-trawler sets were reconciled against the lists 80 vessels licensed for pelagic pair trawling in 2022. All 70 vessels in the GMM-BEST set matched entries in the registry (0 false positives), indicating that 10 licensed vessels were not detected by our behavioral filter, likely due to sparse AIS reporting, inactivity during the observation window, or failure to meet co-occurrence and coordination criteria. This reconciliation and the detailed per-stage accounting (AIS observations, vessel counts, dyad numbers, and *T*distributions) provide a transparent view of data reduction through the analytical pipeline and confirm the internal consistency of the filtering process.

The consistency between the two speed-profile classification schemes was also evaluated to assess robustness. The pelagic vessel sets obtained from the *GMM-BEST* configuration (70 vessels) and the $k = 4$-forced variant (67 vessels) showed a strong overlap of 61 vessels, with 9 unique to *GMM-BEST* and 6 unique to $k = 4$, corresponding to a Jaccard similarity of 0.803. This high degree of agreement demonstrates that the core findings are largely insensitive to the choice of model selection strategy, whether the mixture order is determined by BIC ($k \in \{2, 3, 4\}$) or fixed at $k = 4$, with only a small fraction of vessels exhibiting classification differences between schemes.

Weekly interaction networks were constructed using the FINAL (GMM-BEST) dyads under two operational modes: ALL, which includes all concurrent AIS fixes, and TOW, which considers only periods when both vessels operated within the 2–4 kn towing speed range.

The resulting time series reveal a distinct winter-spring activity pulse (January–March) in the ALL mode (Fig. 6), followed by a near-complete collapse during the national industrial fishing closure (grey band; mid-April to 1 September). Activity resumes briefly after the ban, with a noticeable post-closure resurgence between September and November before declining again in December. Notably, the TOW networks remain almost inactive during the closure but surpass the ALL networks in dyad counts after September, suggesting that most coordinated activity in autumn corresponds to active towing operations. Mean degree and density reach their peaks during weeks with fewer but more interconnected vessels (early September) and decline during periods of widespread fleet activity (late winter). This pattern indicates that the strongest coordination emerges within compact, tightly linked sub-fleets, rather than during peak fleet participation.

To further characterize the coordinated behavior within the FINAL (GMM-BEST) dyads, we analyzed the distribution of the four interaction metrics: Proximity, Directional Heading Synchrony (DI_h), Directional Similarity (DI_θ), and Displacement Similarity (DI_d), under both operational modes (ALL and TOW). Fig. 7 presents the resulting boxplots, illustrating the degree of behavioral coupling across vessel pairs. In the ALL mode, all four metrics exhibit consistently high median values, confirming strong alignment in position and movement among vessels identified as collaborative pairs. Proximity shows slightly greater variability, reflecting occasional divergence in inter-vessel spacing during non-towing intervals. Conversely, in the TOW (2–4 kn) mode, distributions are even more concentrated toward unity, with minimal dispersion across all metrics. This pattern confirms that coordination is most pronounced during active towing operations, where vessels maintain tightly synchronized trajectories and speeds characteristic of pelagic pair trawling.

Across the full observation period, the vessel interaction network remains sparse and fragmented (Fig. 8), reflecting the limited persistence of coordinated pairings within the fleet. The network comprises 70 nodes (vessels) connected by 51 edges, corresponding to an edge density of 0.021, and is partitioned into 22 connected components. A single giant component encompasses approximately 31 % of all vessels (around 22 units), while the remaining nodes appear as isolated dyads or small triads forming short chains. The average degree is modest, at roughly 1.46 partners per vessel, with only a few vessels reaching degrees of 4–5. These higher-degree vessels act as local clusters, forming small but cohesive subgroups within the broader fleet. This topology portrays a loosely connected network, where most vessels engage in short-lived or geographically constrained collaborations, interspersed with a few recurrent “hub” vessels that sustain the structural backbone of coordinated fishing activity.

Component size distributions are strongly right-skewed (Fig. 9), confirming that only a few subnetworks dominate the overall structure. The largest component includes 22 vessels, while subsequent clusters are markedly smaller (for instance, a 7-vessel group), and the vast majority consist of simple two-vessel dyads. This organization reflects a fleet structure composed primarily of stable, recurring pair partnerships operating alongside a single, larger, and more interconnected sub-fleet.

The geographical footprint of these components varies by more than an order of magnitude (Fig. 10). Some groups, such as components ID 10 and ID 5, extend across vast regions of the Black Sea (approximately 130–140 $\times$ 10^3 km^2), while others remain geographically compact (often $< 5 \times 10^3$ km^2). Notably, spatial extent is not directly correlated with group size: certain small dyads operate over wide areas, whereas some of the larger clusters are confined to narrow zones of activity. As noted in the Fig. 10, these surfaces represent convex-hull envelopes of AIS activity and should not be interpreted as the actual trawled areas.

The port connectivity analysis at the component level (Fig. 11) shows

Table 1
Summary of AIS data volume and dyad overlap across sequential filtering stages. Each stage reports the number of AIS position messages (AIS_obs), unique vessels, and unordered vessel pairs (dyads) that co-occurred at least once (≥ 1 concurrent ping). $T_{\text{median}}, T_{q25}, T_{q75}, T_{p10}, T_{p90}$ represent the median, interquartile, and decile statistics of the number of shared timestamps (T) per dyad. Final stages (S3a, S3b) denote pelagic × pelagic dyads classified under the GMM-BEST and $k = 4$-forced schemes, respectively.

Stage No	Stage name	AIS_obs	vessels	dyads	T_median	T_q25	T_q75	T_p10	T_p90
S0	Raw AIS	4,970,928	1011						
S0b	Türkiye-filtered AIS (TC, SPEED≤20, ports excluded)	694,045	708						
S1	Any co-occurrence (dyadic universe)		500	20,039	41	18	80	8	124
S2	Thresholded candidates (0.5/0.5/0.5/0.5)		154	106	43	19	95	6	127
S3a	FINAL (pelagic x pelagic, BEST k∈{2,3,4})		70	51	60	24	103	12	197
S3b	FINAL (pelagic x pelagic, K = 4 forced)		67	49	59	27	103	14.9	197

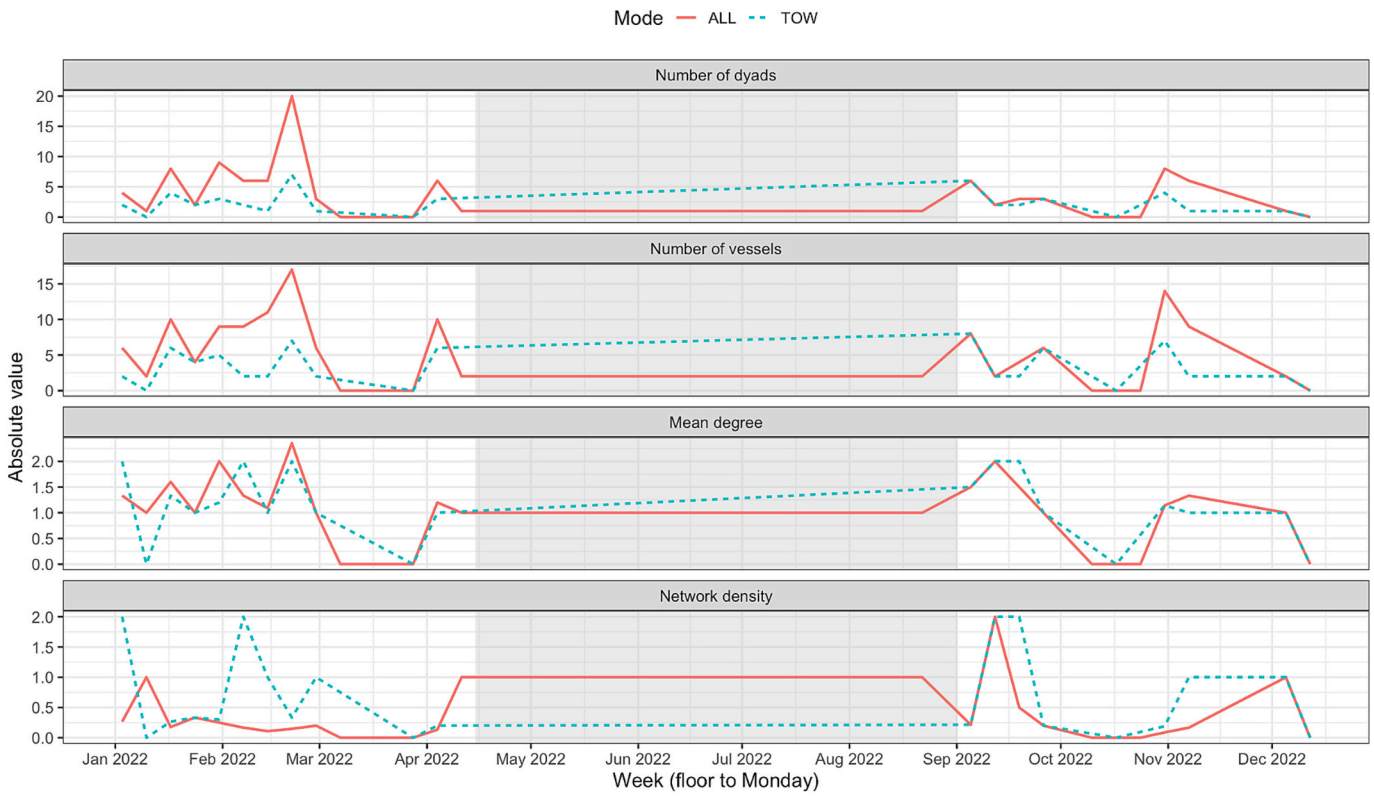

Fig. 6. Weekly network metrics for candidate dyads in ALL (solid line) and TOW (dashed line) modes. Grey shading indicates the national industrial fishing closure (15 April-1 September). Metrics shown per week include the number of dyads, number of vessels, mean degree (average partners per vessel), and network density (proportion of realized links). Axes represent absolute units: dyads (count), mean degree $\bar{k} = 2m/n$(edges per node), and density $\delta = 2m/[n(n-1)]$(unitless; no scaling applied).

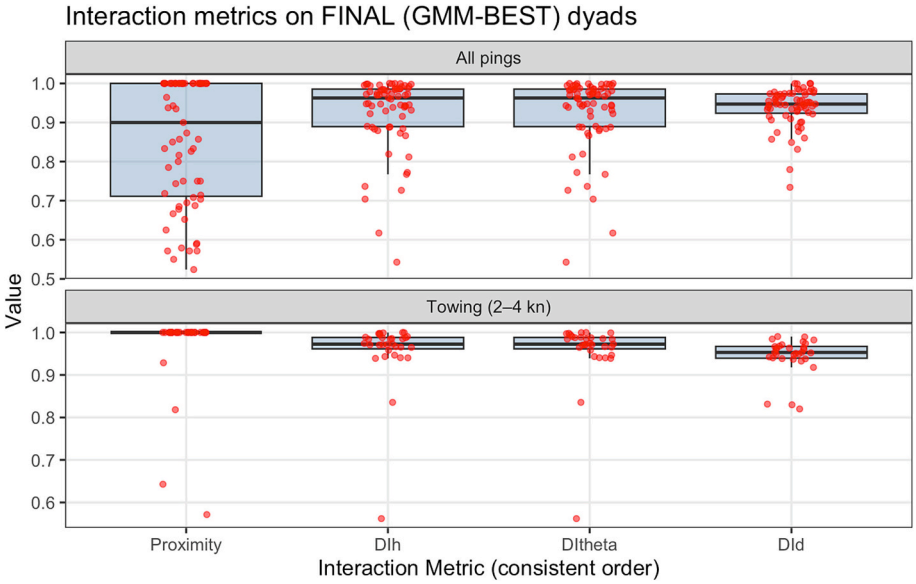

Fig. 7. Boxplots of behavioral coupling metrics (Proximity, DI_h, DI_θ, and DI_d) for identified vessel dyads under the FINAL (GMM-BEST) configuration. Panels compare the distributions for all concurrent AIS fixes (top) and towing-only intervals between 2 and 4 kn (bottom). Red points indicate individual dyad values; boxes show interquartile ranges, and horizontal lines mark medians. (For interpretation of the references to colour in this figure legend, the reader is referred to the web version of this article.)

that coordinated pair-trawling activity is closely aligned with the Turkish coastline, with most component centroids distributed between ~28°E and 37°E. The densest clusters are located along the south-western continental shelf (28–31°E) and the south-central coast (32–34°E), while additional groups are observed near Sinop-Samsun (35–37°E). In the map, colored points represent the centroids of each vessel-network component, black open circles indicate fishing ports, and dashed connectors, where present, link offshore centroids to their

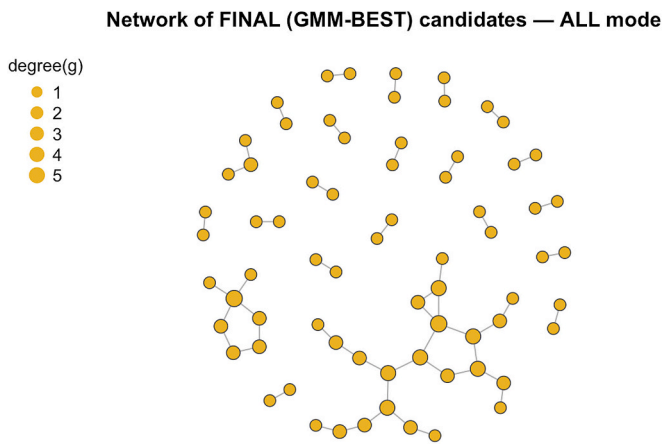

Fig. 8. Aggregated vessel interaction network based on dyadic associations throughout the study period. Nodes are vessels; edges indicate dyads that met the coordination criteria at least once during the study period. Node size encodes degree (number of distinct partners).

nearest port. The resulting spatial configuration highlights a distinct regional segmentation of the fleet and localized port affiliations, consistent with regionally organized pair-trawling practices along the Turkish Black Sea coast.

We quantified directional asymmetry within the FINAL (GMM-BEST) dyads by computing, for each pair, the share of aligned fixes in which vessel 1 lay geometrically ahead of vessel 2 (the "leader score"). The analysis was performed using positional data filtered under three spatial and directional constraints: (i) great-circle distance $\leq$500 m, (ii) absolute heading difference $\leq 10^{\circ}$, and (iii) a geometric-ahead condition derived from vessel orientation vectors. These thresholds were chosen to capture realistic pair-trawling formations while accommodating AIS positional noise and minor course corrections. The thresholds of 500 m and 10° were chosen to capture realistic pair-trawling formations while accounting for AIS positional noise and minor course adjustments. The resulting distributions (Fig. 12) reveal distinct behavioral patterns across operational modes. The red dashed lines at 0.4 and 0.6 serve purely as visual reference markers, representing a $\pm$ 0.10 deviation from perfect symmetry (0.5). Given the minimum sample size of $N \geq 100$ shared observations, a two-sided binomial test with $p_0 = 0.5$ rejects symmetry at approximately α approximately 0.05 when the leader share is $\leq$0.40 or $\geq$ 0.60 (Agresti and Coull, 1998; Wilson, 1927). Thus, these markers approximate statistical asymmetry under small-sample conditions, while formal inference can be verified through exact binomial confidence intervals (CIs).

In the ALL-pings mode, leader scores display a broad, right-skewed distribution (median = 0.481; IQR = 0.333–0.723; p10 = 0, p90 = 1), with a substantial tail of pairs exhibiting persistent directional dominance. Using 0.4 and 0.6 as pragmatic reference markers for asymmetry, 37 % of dyads fall at or below 0.4 (balanced or follower-leaning behavior), while 29.6 % are at or above 0.6 (leader-leaning).

In contrast, the TOWING-only subset (N = 33) is more tightly centered around parity (median = 0.50; IQR = 0.333–0.60; p10 = 0.029, p90 = 0.893), with 36.4 % $\leq$ 0.4 and 27.3 % $\geq$ 0.6. This narrowing in distribution during towing phases aligns with operational constraints: when towing, vessels must maintain an approximately orthogonal net alignment, which naturally limits sustained directional hierarchy. The broader spread observed in the ALL-pings mode likely reflects steaming or maneuvering intervals, during which one vessel temporarily advances to coordinate upcoming trawling operations.

In the ALL-pings analysis, the RQA metrics reveal strong and sustained behavioral coupling across the fleet (Fig. 13). Both determinism (DET) and laminarity (LAM) cluster at high values, reflecting long, repeatable stretches of co-movement throughout the year that encompass both steaming and fishing phases. The recurrence rate (RR) assumes moderate and broadly distributed values, indicating that vessels frequently, but not continuously, revisit similar joint speed states. Meanwhile, entropy (ENTR) remains low to moderate, suggesting that recurrence structures are relatively simple and governed by a limited number of repeating coordination patterns, rather than by highly complex or chaotic transitions.

When the analysis is restricted to TOWING-only intervals, the overall dynamic becomes more constrained. The RR values concentrate in the single-digit to low-teen range, while DET and LAM both decline to mid-range levels, consistent with shorter and more intermittent periods of tight coupling when the net is deployed. The persistence of moderate ENTR values further indicates that, even during active towing, coordination typically alternates among a small set of stable behavioral regimes rather than exhibiting highly variable or irregular patterns.

In the ALL mode, nearly all dyads (48 of 51; 94.1 %) exhibited at least one Intermittent Coordination Window (ICW), with a median cumulative coordination time of 15.25 h (IQR 3.38–81.25 h). Under the

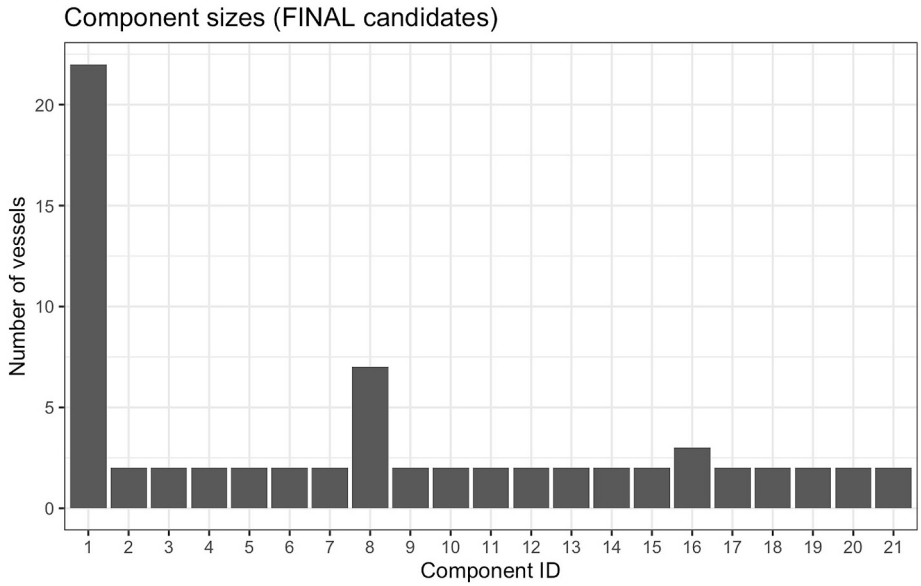

Fig. 9. Number of vessels assigned to each network component. Component IDs are aligned with those in Fig. 3.

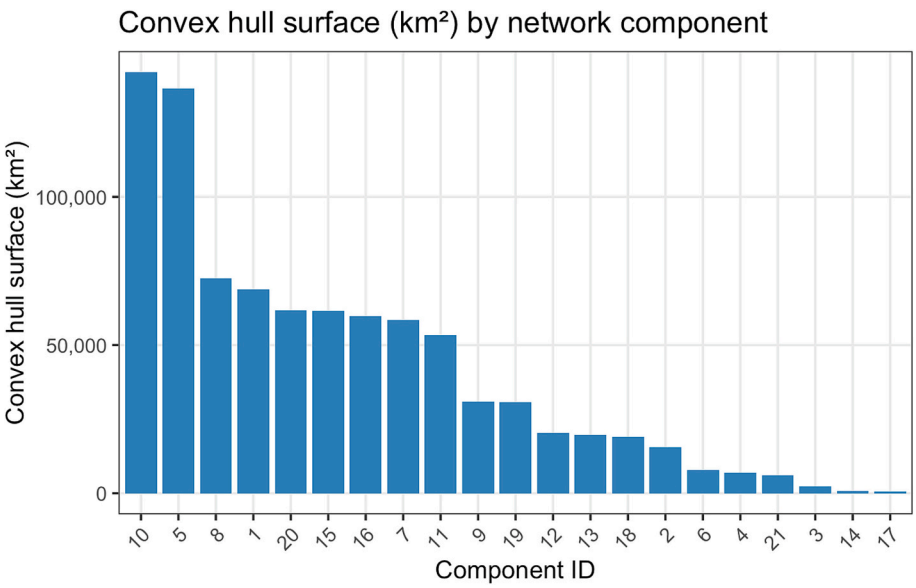

Fig. 10. Spatial area (km^2) covered by each vessel network component identified through connected component analysis. Component ID labels are sorted by decreasing spatial extent.

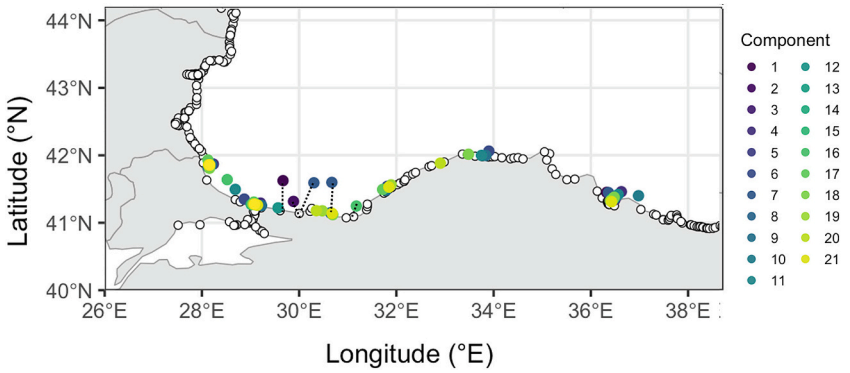

Fig. 11. Ports are shown as neutral grey circles, vessel points are colored by component ID, and straight lines connect each component centroid to its nearest port (by great-circle distance), illustrating the spatial linkage between operational zones and landing sites.

stricter TOW mode, where both vessels were required to be simultaneously within the towing speed band (2–4 kn), 30 dyads (58.8 %) showed ICWs, with a similar median duration of 15.0 h (IQR 3.0–38.5 h). As illustrated in Fig. 14, heatmaps of cumulative ICW duration per dyad reveal pronounced heterogeneity across the fleet: while many pairs exhibit only brief or occasional coordination, a smaller subset demonstrates sustained and recurrent coupling over extended periods. The reduction in coverage from ALL to TOW is expected, as the simultaneous towing requirement shortens temporal overlaps and excludes non-fishing transits or staging phases.

The hex-binned density plots of pairwise separation versus speed difference further clarify these behavioral regimes (Fig. 15). During TOW, the density is sharply concentrated within 0–1000 m of separation and Δspeed <0.5 kn, a signature of tight spatial and kinematic coupling characteristic of active pair trawling. In contrast, the ALL mode displays the same dense core but is accompanied by a long, diffuse tail extending up to ~ 5 km in distance and ~ 10 kn in speed difference, reflecting looser coordination during transit, searching, or repositioning maneuvers.

Taken together, these patterns reinforce the interpretation that true pair-trawling operations are defined by minimal separations and closely matched speeds, whereas the broader ALL dataset encompasses additional operational behaviors that contribute to a more diffuse background of apparent coordination.

4. Discussion and conclusion

Since the introduction of VMS in 2006, valuable insights into fishing patterns and fleet behavior have been derived from vessel position data. This trend accelerated after 2014, when the availability of large-scale AIS big data streams enabled broader analyses of fleet dynamics. Early approaches to fishing activity detection primarily relied on vessel speed and heading to distinguish fishing from non-fishing behavior and to filter noisy positional data (Campanis, 2008). Subsequent developments introduced statistical analyses of speed distributions tailored to specific gear types and fishing techniques (Ferrà et al., 2018; Natale et al., 2015; Vespe et al., 2016). These gear-specific models typically represent vessel tracks as first-order Markov processes or density-based spatial clustering application with noise, that, while limited in generalizability, perform well for classifying activity within targeted fleets (Joo et al., 2013; Nesdoly et al., 2023; Pulcinella et al., 2023; Vermard et al., 2010;). More recently, progress in machine learning, deep learning and high-resolution fisheries informatics further improved cross-fleet classification of fishing activity (de Souza et al., 2016) and gear identification (Kim and Lee, 2020; Kroodsma et al., 2018; Taconet et al., 2019), demonstrating the capability of AIS-based models to classify vessel

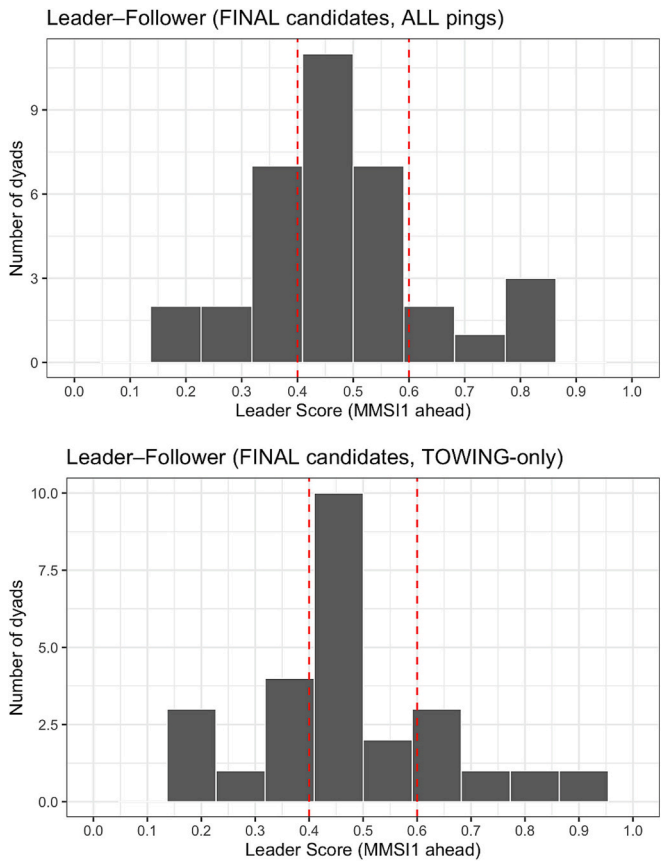

Fig. 12. Distribution of leader scores among dyadic vessel pairs. Leader scores represent the proportion of time a vessel (MMSI1) was spatially ahead of its partner, indicating directional dominance.

activity and estimate fishing effort with unprecedented accuracy (Galparsoro et al., 2024; Henriques et al., 2024).

Despite these advances, collective behavior among fishers has received far less attention than individual movement patterns (Joo et al., 2021). Characterizing this collective behavior can provide valuable inputs for improving movement models and designing more effective management measures (Gezelius, 2007; Rijnsdorp et al., 2011; Salas and Gaertner, 2004;). Recent work by Lee et al. (2025) addressed this challenge from a single-vessel perspective, using voyage data recorder (VDR) tracks, expert annotations, and dockside landings to derive gear- and tonnage-specific towing-speed criteria for six Taiwanese trawl gears. Their model achieved high accuracy for bottom trawls and moderate performance for midwater gears, ultimately linking vessel effort to spatial catch distribution. This represents an important contribution toward the single-vessel, gear-aware classification of fishing activity.

In contrast, our study shifts the analytical focus from single-vessel labeling to interaction-level inference of cooperative fishing behavior. We applied Gaussian Mixture Models for speed-profile classification and detection of potential pelagic trawling behavior, followed by a suite of complementary techniques (such as dyadic movement similarity, fleet profiling, network topology, temporal coordination windows, recurrence dynamics, and direction-based leadership analysis) to focus on their particular collective behavior and reveal a well-structured system of coordinated vessel partnerships.

A complementary perspective is provided by Dağtekin et al. (2021), who analyzed the productive efficiency of the Black Sea pelagic trawl fleet using stochastic frontier analysis (SFA). Our results, focused on behavioral and structural coordination, could enrich such production models by supplying quantitative indicators of cooperation intensity, dyad persistence, and network cohesion. Conversely, SFA-derived efficiency scores could be used to stratify our coordination networks, testing whether more efficient vessels tend to act as central nodes or maintain more stable partnerships.

It is important to note that the towing (2–4 kn) and steaming (6–10 kn) speed thresholds applied in our framework were derived from and validated within known vessels of the Turkish Black Sea fleet. While consistent with prior AIS-based fisheries studies, they reflect local operational characteristics such as vessel size, gear type, and hydrodynamic conditions. In other regions, these parameters should be recalibrated or adapted to account for differences in vessel performance and fishing practices.

In 2022, 80 vessels were featured with midwater pair-trawling, of which 70 were correctly classified by our AIS-based algorithm. The discrepancy can be attributed to gear-switching behavior, which is known to occur unofficially although legally restricted to one annual change. This behavior result in behavioral inconsistencies and obscure pelagic trawling signatures in AIS trajectories.

Although official registries lack harbor information, spatial analysis showed strong alignment between classified vessels and ports locally known to host pelagic trawlers. Our assumption that coordinated pair configurations are unique to pelagic trawlers was supported by Turkish Black Sea fleet records showing no evidence of pair operations among bottom otter trawlers, whether artisanal or industrial. Interestingly, vessels classified as “other” based on speed profiles were mostly purse seiners, whose coordinated behaviors (including joint searching or offloading to auxiliary vessels) differ from true operational dyads. Overall, these results validate our rule-based framework, which detects synchronized movement patterns to infer cooperative pair-trawling behavior.

Following our proposed framework, the filtering pipeline, which reduced 20,039 unordered co-occurrence pairs to a final set of 51 pelagic-only dyads connecting 70 vessels under the GMM-BEST scheme, demonstrated that simple co-location and movement-similarity filters tend to capture numerous incidental associations. Applying speed-profile labeling through BIC-selected Gaussian mixture models ($k \in \{2,3,4\}$) further refined the thresholded candidates from 106 to 51, highlighting the importance of integrating vessel-type classification into dyadic analyses to reliably identify genuine pelagic pair-trawling collaborations (McHugh et al., 2022; Oliver et al., 2023).

Consistent with previous methodological studies on vessel speed distributions using mixture models (Poos et al., 2020), our implementation provided a statistically robust means of distinguishing between steaming and towing behaviors. This strengthens the reproducibility of our analytical framework and aligns it with established standards in fisheries informatics. At the network level, the aggregated graph remains sparse (edge density = 0.021), fragmenting into 22 components, and with a giant component encompassing roughly 31 % of all vessels. The spatial extent of these components varies markedly, from compact operational areas ($<5 \times 10^3$ km^2) to broad footprints spanning up to approximately 1.4×10^5 km^2. The resulting port-connectivity patterns reveal strong regional structuring along the south-western and south-central Turkish shelf. This modularity is consistent with other pair-based fisheries, where spatially cohesive subgroups reflect both practical constraints (such as gear compatibility, home-port proximity) and alliance-building dynamics (Joo et al., 2021; Strandburg-Peshkin et al., 2015). Collectively, these results suggest that most partnerships are shaped by efforts to minimize steaming distances and coordinate gear handling efficiently, whereas a smaller number of wide-footprint components likely follow migratory shoals across broader fishing grounds.

The observed vessel-pair network was markedly fragmented, with most dyadic relationships forming small, disconnected clusters, while a few vessels acted as hubs maintaining cohesion across the broader fleet. This dual configuration, marked by the coexistence of numerous dyadic cliques and a limited number of central nodes, reflects patterns

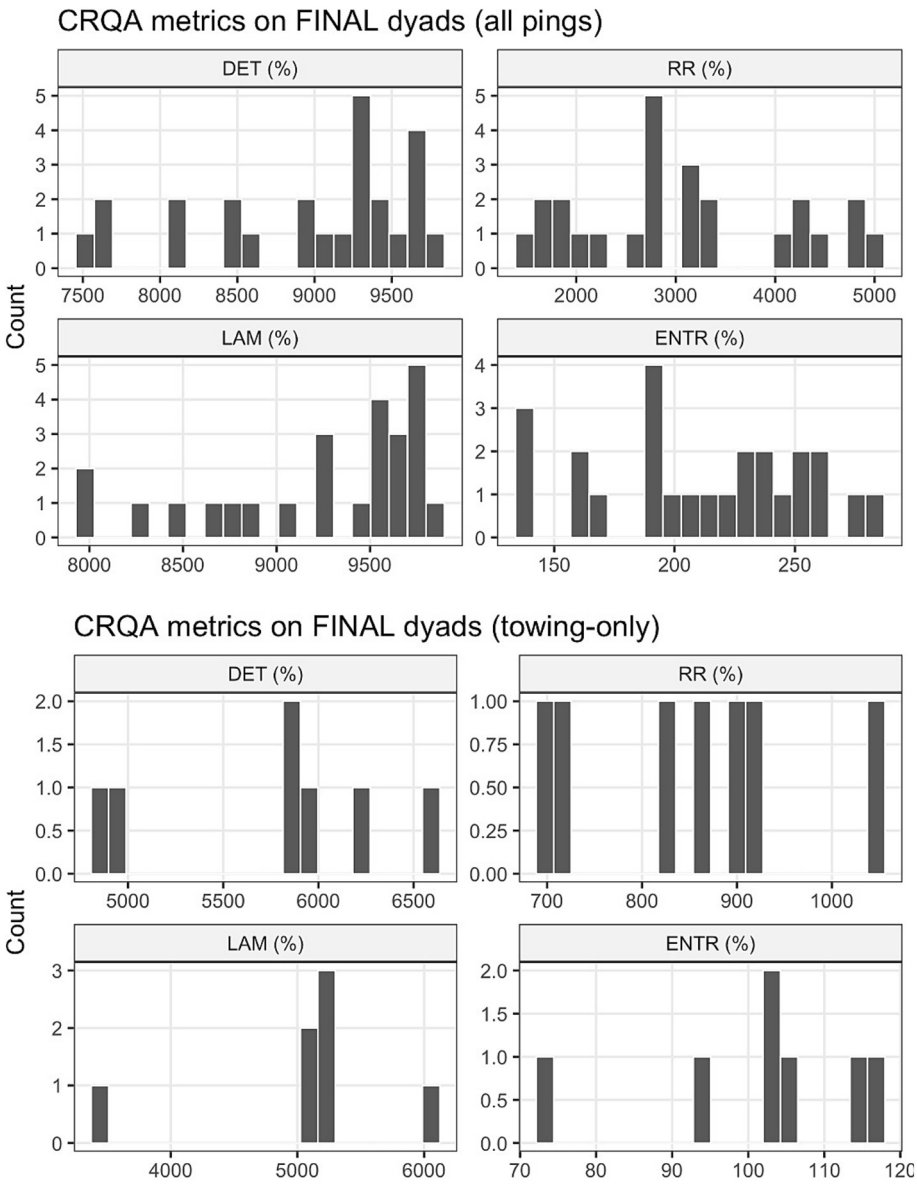

Fig. 13. Histogram distributions of recurrence quantification metrics derived from vessel movement time series. Top-left: Determinism (DET), Top-right: Recurrence Rate (RR), Bottom-left: Laminarity (LAM), Bottom-right: Entropy (ENTR).

documented in other fisheries social networks, where both opportunistic, short-lived collaborations and more stable alliances coexist (Joo et al., 2018; Nogueira et al., 2025). The presence of high-degree vessels suggests that some skippers or vessels possess characteristics (e.g., extensive local knowledge, superior gear performance, or reputational standing) that attract repeated partnerships, thereby reinforcing their centrality and influence within the network (Hilborn, 1985; Salas and Gaertner, 2004). These hub vessels likely play a crucial role in enhancing coordination efficiency and facilitating information exchange, much like keystone actors that shape collective movement in animal groups (Strandburg-Peshkin et al., 2015) and in community-led fisheries management networks (Munguia-Vega et al., 2022). Their influence likely extends beyond operational coordination in paired trawling, suggesting that targeted interventions such as training initiatives or gear upgrades focused on these central vessels could yield cascading benefits across the broader fleet.

Spatial component analysis revealed substantial heterogeneity in the operational footprints of dyadic clusters, ranging from broad areas exceeding 70,000 km^2 to highly localized zones under 5000 km^2. This variability in spatial extent likely reflects differences in target species distribution, vessel range, and economic incentives (Dağtekin et al., 2021). Wide-ranging components may correspond to mobile sprat or anchovy fisheries during periods of dispersed schooling, whereas localized clusters likely target dense horse mackerel aggregations near coastal features (Erdem and Özdemir, 2008), highlighting the coexistence of exploratory and more stationary coastal strategies within the pelagic fleet.

ICW analysis identified a minority of dyads with exceptionally high counts (> 10,000 windows) of sustained coordination, confirming that pair trawling involves repeated short-term alignments both in space (less than 1852 m) and speed (below 1 knot), consistent with established behavioral protocols in collective movement systems (Joo et al., 2018; Long et al., 2014). The tight clustering of ICW events near the lower thresholds supports both the parameters' choice and the ecological realism of the detected coordination windows. ICW typically spanned three to six consecutive fixes (approximately 30–60 min), aligning with the stop-start foraging rhythms described in shoaling fish and bird flocks (Long et al., 2014; Strandburg-Peshkin et al., 2015). Sensitivity tests confirmed that shorter windows capture brief but intense coordinated events, while longer ones tended to include transit or non-fishing phases,

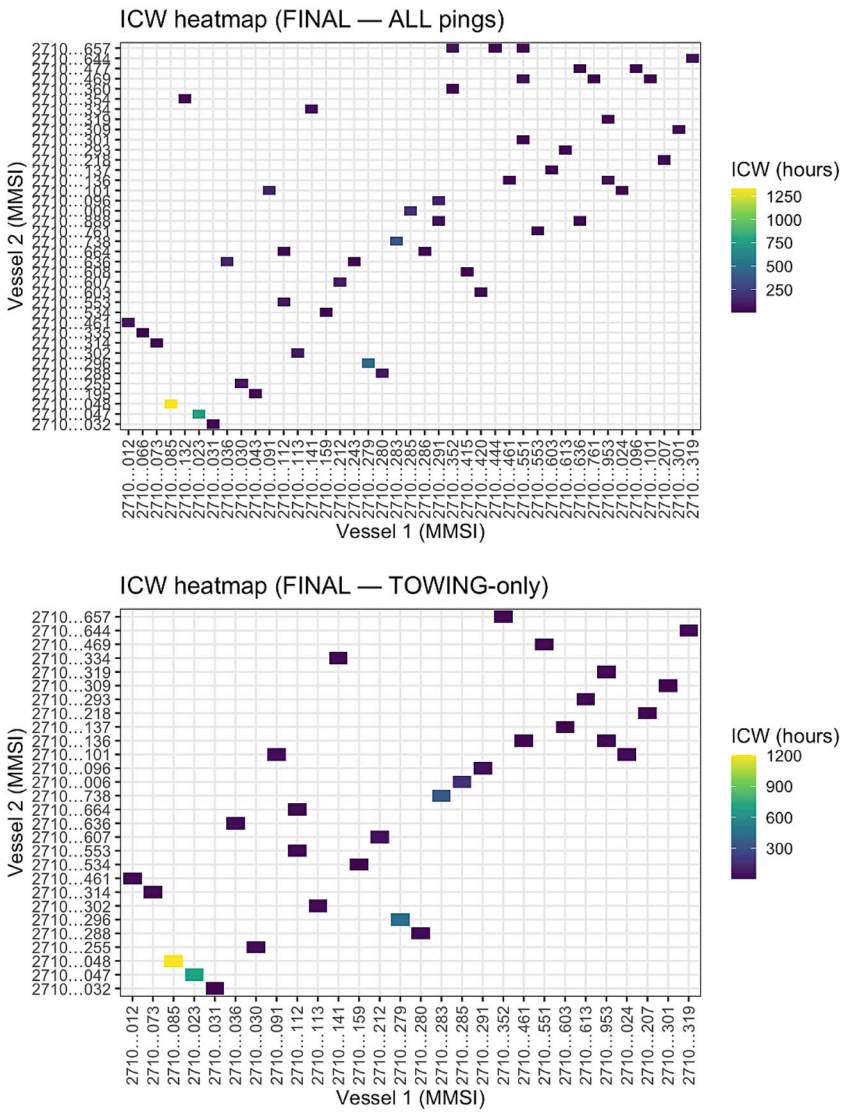

Fig. 14. Intermittent Coordination Window (ICW) frequency heatmap showing the number of coordinated time windows detected between all vessel pairs. MMSI numbers have been anonymized to enhance readability. The colour scale indicates the total number of ICWs, with yellow representing the highest frequency. (For interpretation of the references to colour in this figure legend, the reader is referred to the web version of this article.)

underscoring that fine temporal resolution is essential for distinguishing cooperative behavior in AIS-derived networks.

The RQA of paired speed time series added a complementary perspective on behavioral consistency. High determinism (DET > 90 %) and laminarity (LAM > 90 %), combined with low RR and moderate entropy (ENTR value of around 2–4), depicted a clear picture of stable and repeatable operational dynamics among coordinated vessel pairs, likely optimized for gear performance and fuel efficiency. In dynamical systems terms, these patterns suggest that vessel speed profiles follow predictable and stable trajectories sampling only a narrow subset of speed states (Marwan et al., 2007). Once established, coordination persists through long, uninterrupted sequences consistent with protocol-driven and synchronized towing, while moderate entropy values suggest structured variability rather than random behavior (Coco and Dale, 2014; Shockley et al., 2003). These findings confirm that pelagic pair trawling operates through deliberate and repeatable coordination patterns that balance stability with adaptive responsiveness.

Leader-follower scoring revealed that most vessel dyads operated in spatially balanced configurations, with leadership scores clustered near zero. However, a nontrivial subset exhibited marked asymmetry (score > 0.4), suggesting that in certain partnerships, one vessel often occupied the forward position during coordinated movements. In pelagic pair trawling, persistent leadership likely reflects differences in navigational skill, local ecological knowledge, or tactical control over net positioning-attributes often linked to skipper experience or vessel outfitting. The lead vessel commonly assumes responsibility for locating fish schools (using echosounders and other fish-finding technologies) and guiding net deployment to maximize encounters with dense schools, thereby improving catch efficiency for the pair (Coco and Dale, 2014). The emergence of such spatial hierarchies, even within a nominally cooperative activity, underscores the subtle structuring of authority within fishing partnerships and suggests that not all dyads operate under perfectly reciprocal dynamics. These asymmetries may influence catch distribution, decision-making power, and conflict potential within long-term collaborations, as well as affect the efficiency of joint search strategies in a highly dynamic marine environment.

Finally, both RQA and ICW analyses bridge fisheries analytics with the broader literature on coordinated systems. Although originally developed to study animal and human collective motion (Marwan et al., 2007), these methods adapt effectively to vessel interactions shaped by operational constraints such as towing speeds, safety distances, and regulatory closures (Pallotta et al., 2013; Tu et al., 2018).

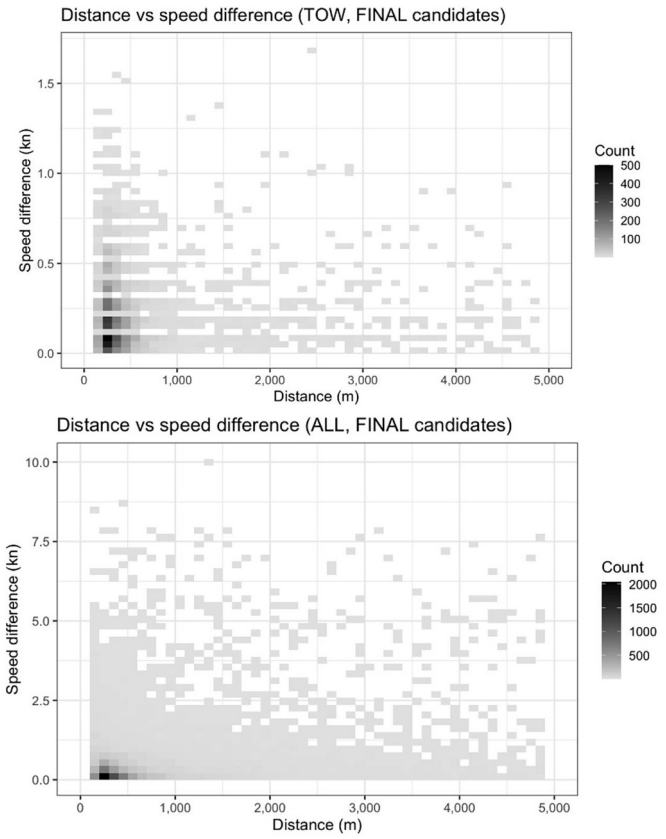

Fig. 15. Scatterplot depicting the coordination conditions during all detected ICWs across vessel dyads. Each point represents a single ICW window characterized by its distance (meters) and absolute speed difference (knots).

Recent comparisons indicate that presumptions embedded in Artificial Intelligence (AI)-derived fishing activity products can substantially overestimate actual fishing activity, underscoring the need for transparent verification and explicit methodological framework (Hintzen et al., 2025). Our approach addresses this by treating each vessel pair as a coupled, human-operated system governed by seamanship, gear dynamics, and regulatory constraints rather than purely mechanical or biological factors. From a technical perspective, several adaptations were introduced to tailor the RQA and ICW frameworks to vessel behavior. Towing-speed series were standardized (z-scored) and aggregated into 10-min bins to provide a consistent, unitless recurrence radius across vessels (Marwan et al., 2007). RQA was then applied in two complementary modes (ALL pings and TOWING-only) to separate transit co-movement from coordinated fishing activity, while short ICW windows of about 30 min captured operational cycles typical of trawl set-and-haul sequences (Andrienko and Andrienko, 2012). All detected RQA/ICW patterns were validated against known AIS indicators of fishing, such as stable towing speeds (2–4 kn), sustained proximity, and spatial distributions around ports and established fishing grounds (Pallotta et al., 2013; Tu et al., 2018).

These adaptations build on two well-established research lines: trajectory mining and co-movement analysis in maritime systems, which uses AIS data increasingly clustered/networked and proximity and speed filters to infer coordinated intent (Andrienko and Andrienko, 2012; Jeung et al., 2010), and recurrence analysis originally developed for nonlinear, noisy time series but now widely applied to human and engineered coordination (Marwan et al., 2007). Together, these approaches justify using RQA to quantify predictability (DET), intermittency (LAM), complexity (ENTR), and prevalence (RR) of vessel dyads, and of ICW to identify short, repeated intervals of tight spatial-kinematic alignment characteristic of pair trawling in formation (Jeung et al., 2010; Pallotta et al., 2013). These methodological adaptations translate principles originally developed for biological coordination into the operational domain of human-directed fishing systems, preserving the analytical rigor of recurrence analysis while aligning its parameters with maritime behavioral dynamics. This approach remains consistent with established AIS-based co-movement studies and with best practices for applying recurrence methods to non-stationary behavioral data (Andrienko and Andrienko, 2012; Marwan et al., 2007; Tu et al., 2018).

Overall, our findings show that pelagic pair trawling in the Black Sea operates through neither purely ad-hoc nor fully centralized dynamics, but rather as a mosaic of small, stable partnerships interspersed with transient collaborations. From a management perspective, identifying the small subset of highly coordinated and spatially extensive dyads could inform targeted monitoring, fuel-efficiency incentives, or spatial management measures (e.g., dynamic area closures) aimed at reducing ecological impacts while preserving economic viability (Galdelli et al., 2019; Salas and Gaertner, 2004).

Although developed for the Turkish Black Sea pelagic fleet, our framework, combining dyadic proximity thresholds, trajectory-based coordination metrics, and speed-profile classification, remains modular and transferable to other cooperative fisheries. Similar dynamics observed in midwater pair-trawling in the Adriatic Sea (Russo et al., 2015) highlight its broader applicability. By recalibrating coordination thresholds and classification parameters to reflect regional gear types, licensing structures, and AIS usage patterns, our analytical pipeline could be readily providing a strong foundation for comparative informatics research across diverse cooperative fisheries. In contrast, fisheries where coordinated operations rely on non-spatial synchronization, such as tuna purse seine operations or dark fleet activities, would require integration with radio-frequency monitoring, VMS, or observer-based data. In regions affected by substantial AIS disruption or intentional shutdowns, coupling the framework with trajectory imputation or deep learning-based interpolation (Galdelli et al., 2025) could further enhance detection robustness.

Future work will extend the analysis across multiple years of AIS data to assess the temporal stability of vessel partnerships and coordination patterns. Applying the framework to other regions will test its robustness under diverse environmental and operational contexts. Integration of complementary data sources such as VMS, logbooks, and environmental variables will improve validation and predictive capability. Further methodological developments, including deep learning and hierarchical mixture models, will refine behavioral classification and explore links between coordination dynamics, efficiency, and management outcomes. Together, these efforts will broaden the framework's applicability and reinforce its role as a comparative tool for sustainable fleet monitoring.

CRediT authorship contribution statement

Taner Yıldız: Writing – review & editing, Writing – original draft, Visualization, Validation, Software, Resources, Project administration, Methodology, Investigation, Funding acquisition, Formal analysis, Data curation, Conceptualization. **Alessandro Galdelli:** Writing – review & editing, Writing – original draft, Visualization, Validation, Software, Methodology, Investigation, Formal analysis. **Nurdan Cömert:** Writing – review & editing, Writing – original draft, Visualization, Methodology, Investigation, Formal analysis, Data curation, Conceptualization. **Adriano Mancini:** Writing – review & editing, Writing – original draft, Validation, Software, Investigation, Formal analysis. **Anna Nora Tassetti:** Writing – review & editing, Writing – original draft, Visualization, Validation, Methodology, Investigation.

Declaration of competing interest

The authors declare that they have no known competing financial interests or personal relationships that could have appeared to influence the work reported in this paper.

Acknowledgments

This study was supported by Istanbul University BAP Scientific Research Projects Coordination Unit. Project number: FBA-2023-39669. A.G and A.N.T acknowledge funding by the National Recovery and Resilience Plan (NRRP), Mission 4 Component 2 Investment 1.4 - Call for tender No. 3138 of 16 December 2021, rectified by Decree n.3175 of 18 December 2021 of Italian Ministry of University and Research funded by the European Union – NextGenerationEU; Award Number: Project code CN_00000033, Concession Decree No. 1034 of 17 June 2022 adopted by the Italian Ministry of University and Research, Project title "National Biodiversity Future Center - NBFC". The authors would like to acknowledge Dr. Gagan Narang, Ph.D. for his valuable assistance in reviewing and proofreading the manuscript.

Data availability

The R code for statistical analysis and visualization is available at https://github.com/Galdo89/Pelagic-trawl-in-the-Black-Sea

References

Agresti, A., Coull, B.A., 1998. Approximate is better than "exact" for interval estimation of binomial proportions. Am. Stat. 52 (2), 119–126. https://doi.org/10.2307/2685469.

Akoğlu, E., 2023. Ecological indicators reveal historical regime shifts in the Black Sea ecosystem. PeerJ 11, e15649. https://doi.org/10.7717/peerj.15649.

Akoğlu, E., Salihoglu, B., Libralato, S., Oguz, T., Solidoro, C., 2014. An indicator-based evaluation of Black Sea food web dynamics during 1960–2000. J. Mar. Syst. 134, 113–125. https://doi.org/10.1016/j.jmarsys.2014.02.010.

Andrienko, N., Andrienko, G., 2012. Visual analytics of movement: an overview of methods, tools and procedures. Inf. Vis. 12 (1), 3–24. https://doi.org/10.1177/1473871612457601.

Ayaz, A., Özekinci, U., Kınacığil, H.T., 2000. Karadeniz' de ortasu trol balıkçılığı üzerine bir araştırma. Ege Üniversitesi Su Ürünleri Dergisi, Cilt 95–108. No 17, Sayı:1-2.

Barabási, A.-L., 2016. Network Science (Chapter 3). Cambridge University Press. https://doi.org/10.1063/PT.3.3526.

Brandoli, B., Raffaeta, A., Simeoni, M., Adibi, P., Bappee, F., Pranovi, F., Rovinelli, G., Russo, E., Silvestri, C., Soares, A., 2022. From multiple aspect trajectories to predictive analysis: a case study on fishing vessels in the northern Adriatic Sea. GeoInformatica 26. https://doi.org/10.1007/s10707-022-00463-4.

Campanis, G., 2008. Advancements in VMS data analyses. NAFO Annual Report for 2008. Northwest Atlantic Fisheries Organization. https://www.nafo.int/Portals/0/PDFs/ar/ar08.pdf?ver=2016-02-10-101458-760.

Cheng, X., Wang, J., Chen, X., et al., 2025. Attention-enhanced and integrated deep learning approach for fishing vessel classification based on multiple features. Sci. Rep. 15, 8642. https://doi.org/10.1038/s41598-025-88158-2.

Coco, M.I., Dale, R., 2014. Cross-recurrence quantification analysis of categorical and continuous time series: an R package. Front. Psychol. 5, 510. https://doi.org/10.3389/fpsyg.2014.00510.

Coco, M.I., Monster, D., Leonardi, G., Dale, R., Wallot, S., 2021. Unidimensional and multidimensional methods for recurrence quantification analysis with crqa. R J. 13 (1). https://doi.org/10.32614/RJ-2021-062.

Coro, G., Ellenbroek, A., Pagano, P., 2021. An Open Science approach to infer fishing activity pressure on stocks and biodiversity from vessel tracking data. Eco. Inform. 64, 101384. https://doi.org/10.1016/j.ecoinf.2021.101384.

Coro, G., Tassetti, A.N., Armelloni, E.N., Pulcinella, J., Ferrà, C., Sprovieri, M., Trincardi, F., Scarcella, G., 2022. COVID-19 lockdowns reveal the resilience of Adriatic Sea fisheries to forced fishing effort reduction. Sci. Rep. 12, 1052. https://doi.org/10.1038/s41598-022-05142-w.

Csardi, G., Nepusz, T., 2006. The igraph software package for complex network research. InterJournal Complex Syst. 1695, 1–9.

Dağtekin, M., Uysal, O., Candemir, S., Genç, Y., 2021. Productive efficiency of the pelagic trawl fisheries in the southern Black Sea. Reg. Stud. Mar. Sci. 45, 101853. https://doi.org/10.1016/j.rsma.2021.101853.

de Souza, E.N., Boerder, K., Matwin, S., Worm, B., 2016. Improving fishing pattern detection from satellite AIS using data mining and machine learning. PloS One 11 (7), e0158248. https://doi.org/10.1371/journal.pone.0158248.

Erdem, Y., Özdemir, S., 2008. Fishing of some pelagic species by pairly midwater trawl in Blacksea coast, Anadolu. J. Agric. Sci. 23 (2), 78–82 ref. 14.

Ferrà, C., Tassetti, A.N., Grati, F., Pellini, G., Polidori, P., Scarcella, G., Fabi, G., 2018. Mapping change in bottom trawling activity in the Mediterranean Sea through AIS data. Mar. Policy 94, 275–281. https://doi.org/10.1016/j.marpol.2017.12.013.

Ferrà, C., Tassetti, A.N., Armelloni, E.N., Galdelli, A., Scarcella, G., Fabi, G., 2020. Using AIS to attempt a quantitative evaluation of unobserved trawling activity in the Mediterranean Sea. Front. Mar. Sci. 7, 580612. https://doi.org/10.3389/fmars.2020.580612.

Fisher, N.I., 1993. Statistical Analysis of Circular Data. Cambridge University Press. https://doi.org/10.1017/CBO9780511564345.

Galdelli, A., Mancini, A., Tassetti, A.N., Ferrà Vega, C., Armelloni, E., Scarcella, G., Fabi, G., Zingaretti, P., 2019. A cloud computing architecture to map trawling activities using positioning data. In: Proceedings of the ASME 2019 International Design Engineering Technical Conferences and Computers and Information in Engineering Conference. Volume 9: 15th IEEE/ASME International Conference on Mechatronic and Embedded Systems and Applications. Anaheim, California, USA. August 18–21, 2019. ASME. https://doi.org/10.1115/DETC2019-97779. V009T12A035.

Galdelli, A., Narang, G., Tomassini, S., et al., 2025. Data imputation in large and small-scale spatiotemporal time series gaps using BackForward bi-LSTM. J. Big Data 12, 115. https://doi.org/10.1186/s40537-025-01163-0.

Galparsoro, I., et al., 2024. Predicting important fishing grounds for the small-scale fishery, based on automatic identification system records, catches, and environmental data. ICES Journal of Marine Science 81 (3), 453–469. https://doi.org/10.1093/icesjms/fsae006.

Gezelius, S.S., 2007. The social aspects of fishing effort. Hum. Ecol. 35, 587–599. https://doi.org/10.1007/s10745-006-9096-z.

Gillis, D.M., et al., 2021. Association networks in the Dutch offshore beam trawl fleet: their predictors and relationship to vessel performance. Can. J. Fish. Aquat. Sci. 78 (7), 924–942. https://doi.org/10.1139/cjfas-2019-0353.

Godø, O.R., Pennington, M., Vølstad, J.H., 1990. Effect of tow duration on length composition of trawl catches. Fish. Res. 9 (2), 165–179. https://doi.org/10.1016/0165-7836(90)90062-Z.

Gümüş, A., Zengin, M., 2011. 2000'li yılların başında Samsun balıkçılığının durumu: Çöken demersal stoklarına karşılık alternatife arayışlar. In: Samsun Sempozyumu. Governorship of Samsun, Samsun, Türkiye, pp. 315–333.

Harati-Mokhtari, A., Wall, A., Brooks, P., Wang, J., 2007. Automatic Identification System (AIS): data reliability and human error implications. J. Navig. 60 (3), 373–389. https://doi.org/10.1017/S0373463307004298.

Henriques, N., et al., 2024. Let's measure it: an approach of high-resolution estimates of bottom fixed net fishing effort at national level. Fish. Res. 273, 107118. https://doi.org/10.1016/j.fishres.2024.107118.

Hijmans, R., 2024. geosphere: Spherical Trigonometry. R Package Version 1.5-20. https://github.com/rspatial/geosphere.

Hilborn, R., 1985. Fleet dynamics and individual variation: why some people catch more fish than others. Can. J. Fish. Aquat. Sci. 42 (1), 2–13. https://doi.org/10.1139/f85-001.

Hintzen, N.T., Bastardie, F., Beare, D., Piet, G.J., Ulrich, C., Deporte, N., Egekvist, J., Degel, H., 2012. VMStools: open-source software for the processing, analysis and visualization of fisheries logbook and VMS data. Fish. Res. 115-116, 31–43. https://doi.org/10.1016/j.fishres.2011.11.00.

Hintzen, N.T., Brigden, K., Kaastra, H., Mackinson, S., Pastoors, M.A., van de Pol, L., 2025. Bias in global fishing watch AIS data analyses results in overestimate of Northeast Atlantic pelagic fishing impact. ICES J. Mar. Sci. 82 (3). https://doi.org/10.1093/icesjms/fsaf033.

Hinz, H., Murray, L.G., Lambert, G.I., Hiddink, J.G., Kaiser, M.J., 2013. Confidentiality over fishing effort data threatens science and management progress. Fish Fish. 14, 110–117. https://doi.org/10.1111/j.1467-2979.2012.00475.x.

Huettmann, F., Arhonditsis, G., 2023. Towards an ecological informatics scholarship that is reflective, repeatable, transparent, and sharable! Eco. Inform. 76, 102132. https://doi.org/10.1016/j.ecoinf.2023.102132.

ITU-R, 2001. Recommendation ITU-R M.1371-1 (Class-A AIS Field Definitions; SOG Resolution; PA flag). https://www.itu.int/dms_pubrec/itu-r/rec/m/R-REC-M.1371-1-200108-S!!PDF-E.pdf.

Jaccard, P., 1901. Étude comparative de la distribution florale dans une portion des Alpes et du Jura. Bull. Soc. Vaudoise Sci. Nat. 37, 547–579. https://doi.org/10.5169/seals-266450.

Jaccard, P., 1908. Nouvelles recherches sur la distribution florale. Bull. Soc. Vaudoise Sci. Nat. 44, 223–270. https://doi.org/10.5169/seals-268384.

Jeung, H., Yiu, M.L., Zhou, X., Jensen, C.S., Shen, H.T., 2010. Discovery of Convoys in Trajectory Databases. arXiv preprint arXiv:1002.0963. https://doi.org/10.48550/arXiv.1002.0963.

Joo, R., Bertrand, S., Tam, J., Fablet, R., 2013. Hidden Markov models: the best models for forager movements? PloS One 8 (8), e71246. https://doi.org/10.1371/journal.pone.0071246.

Joo, R., Salcedo, O., Gutierrez, M., Fablet, R., Bertrand, S., 2015. Defining fishing spatial strategies from VMS data: insights from the world's largest monospecific fishery. Fish. Res. 164, 223–230. https://doi.org/10.1016/j.fishres.2014.12.004.

Joo, R., Etienne, M.P., Bez, N., Mahévas, S., 2018. Metrics for describing dyadic movement: a review. Movement Ecol. 6, 1–17. https://doi.org/10.1186/s40462-018-0144-2.

Joo, R., Bez, N., Etienne, M.P., Marin, P., Goascoz, N., Roux, J., Mahévas, S., 2021. Identifying partners at sea from joint movement metrics of pelagic pair trawlers. ICES Journal of Marine Science 78 (5), 1758–1768. https://doi.org/10.1093/icesjms/fsab068.

Katz, Y., Tunstrøm, K., Ioannou, C.C., Huepe, C., Couzin, I.D., 2011. Inferring the structure and dynamics of interactions in schooling fish. PNAS 108 (46), 18720–18725. https://doi.org/10.1073/pnas.1107583108.

Kim, K.-i, Lee, K.M., 2020. Convolutional neural network-based gear type identification from automatic identification system trajectory data. Appl. Sci. 10 (11), 4010. https://doi.org/10.3390/app10114010.

Knudsen, S., Zengin, M., 2006. Multidisciplinary modelling of Black Sea fisheries: a case study of trawl and sea snail fisheries in Samsun. In: 1st Biannual Scientific Conference Black Sea Ecosystem 2005 and Beyond 8-10 May 2006, Istanbul.

Kroodsma, D.A., Mayorga, J., Hochberg, T., Miller, N.A., Boerder, K., Ferretti, F., Wilson, A., Bergman, B., White, T.D., Block, B.A., Woods, P., Sullivan, B.,

Costello, C., Worm, B., 2018. Tracking the global footprint of fisheries. Science 359 (6378), 904–908. https://doi.org/10.1126/science.aao5646.
Lee, Y., Hsu, W.W., Lee, H., Liao, C., 2025. Enhancing the resolution of fishing dynamics in Taiwan's mixed-trawl fisheries: investigating gear type operation patterns through vessel tracks. Reg. Stud. Mar. Sci. 81. https://doi.org/10.1016/j.rsma.2024.103928.
Letschert, J., Müller, B., Dressler, G., Möllmann, C., Stelzenmüller, V., 2025. Simulating fishery dynamics by combining empirical data and behavioral theory. Ecol. Model. 2025 (501), 111036. https://doi.org/10.1016/j.ecolmodel.2025.111036.
Liu, R.W., Liang, M., Nie, J., Lim, W.Y.B., Zhang, Y., Guizani, M., 2022. Deep learning-powered vessel trajectory prediction for improving smart traffic services in maritime internet of things. IEEE Trans Netw Sci Eng 9 (5), 3080–3094. https://doi.org/10.1109/TNSE.2022.3140529.
Long, J.A., Nelson, T.A., Webb, S.L., Gee, K.L., 2014. A critical examination of indices of dynamic interaction for wildlife telemetry studies. J. Anim. Ecol. 83 (5), 1216–1233. https://doi.org/10.1111/1365-2656.12198.
Maina, I., Kavadas, S., Damalas, D., Pantazi, M., Katsanevakis, S., 2018. Dynamics of trawling effort in the Aegean Sea: investigating the potential of vessel monitoring system (VMS) data. ICES J. Mar. Sci. 75 (6), 2265–2275. https://doi.org/10.1093/icesjms/fsy083, 2018.
Mardia, K.V., Jupp, P.E., 1999. Directional Statistics. In: Series in Probability and Statistics, 1st ed. Wiley. https://doi.org/10.1002/9780470316979.
Marwan, N., Romano, M.C., Thiel, M., Kurths, J., 2007. Recurrence plots for the analysis of complex systems. Phys. Rep. 438 (5–6), 237–329. https://doi.org/10.1016/j.physrep.2006.11.001.
McHugh, M., Oliver, M., Browne, D., Cambell, R., Cosgrove, R., 2022. Assessment of Pair Fishingtowards More Efficient Targeting of Demersal Fish Species. Irish Sea Fisheries Board (BIM) (Fisheries Conservation Report, December 2022. 12 pp.).
Mendo, T., Glemarec, G., Mendo, J., Hjorleifsson, E., Smout, S., Northridge, S., Rodriguez, J., Mujal-Colilles, A., James, M., 2023. Estimating fishing effort from highly resolved geospatial data: focusing on passive gears. Ecol. Indic. 154, 110822, 9p. https://doi.org/10.1016/j.ecolind.2023.110822.
Munguia-Vega, A., Zepeda-Dominguez, J.A., Perez-Alarcon, M.F., Amador-Castro, I.G., Fulton, S., Walther, M., et al., 2022. Social-ecological networks and connectivity within and between two communities of small-scale fishers in Mexico. Ecol. Soc. 27 (1). https://doi.org/10.5751/ES-13055-270124.
Natale, F., Gibin, M., Alessandrini, A., Vespe, M., Paulrud, A., 2015. Mapping fishing effort through AIS data. PloS One 10 (6), e0130746. https://doi.org/10.1371/journal.pone.0130746.
Nesdoly, A., Bone, C., Fraser, M., Serra-Sogas, N., Canessa, R., 2023. Evaluating models for classifying movement of whale-watching vessels. Ecol. Inform. 73 (2023), 101903. https://doi.org/10.1016/j.ecoinf.2022.101903.
Newman, M.E.J., 2010. Networks: An Introduction. Oxford University Press.
Nogueira, B., Torres, A., Moniz, N., Menezes, G.M., 2025. Dynamics of fisheries in the Azores Islands: a network analysis approach. In: Santos, M.F., Machado, J., Novais, P., Cortez, P., Moreira, P.M. (Eds.), Progress in Artificial Intelligence. EPIA 2024. Lecture Notes in Computer Science, vol 14968. Springer, Cham. https://doi.org/10.1007/978-3-031-73500-4_25.
Oliver, M., McHugh, M., Browne, D., Campbell, R., Cooney, R., Cosgrove, R., 2023. Assessment of Pair-fishing Operations in the Irish Demersal Seine Fishery. Irish Sea Fisheries Board (BIM) (Fisheries Conservation Report, March 2023. 11 pp.).
Pallotta, G., Vespe, M., Bryan, K., 2013. Vessel pattern knowledge discovery from AIS data: a framework for anomaly detection and route prediction. Entropy 15 (6), 2218–2245. https://doi.org/10.3390/e15062218.
Pebesma, E., Bivand, R., 2023. Spatial Data Science: With Applications in R. Chapman and Hall/CRC. https://doi.org/10.1201/9780429459016.
Poos, J.J., et al., 2020. Efficiency changes in bottom trawling for flatfish species as a result of the replacement of mechanical stimulation by electric stimulation. ICES Journal of Marine Science 77 (7–8), 2635–2645. https://doi.org/10.1093/icesjms/fsaa126.
Pulcinella, J., Armelloni, E.N., Ferrà, C., Scarcella, G., Tassetti, A.N., 2023. Deep-water red shrimp fishery in the eastern-central Mediterranean Sea: AIS-observed monthly fishing effort and frequency over 4 years. Earth Syst. Sci. Data 15, 809–820. https://doi.org/10.5194/essd-15-809-2023.
Rijnsdorp, A.D., Poos, J.J., Quirijns, F.J., 2011. Spatial dimension and exploitation dynamics of local fishing grounds by fishers targeting several flatfish species. Can. J. Fish. Aquat. Sci. 68 (6), 1064–1076. https://doi.org/10.1139/f2011-032.
Rubbens, P., Brodie, S., Cordier, T., Destro Barcellos, D., Devos, P., Fernandes-Salvador, J.A., Fincham, J.I., Gomes, A., Handegard, N.O., Howell, K., Jamet, C., Kartveit, K.H., Moustahfid, H., Parcerisas, C., Politikos, D., Sauzède, R., Sokolova, M., Uusitalo, L., Van den Bulcke, L., Van Helmond, A.T.M., Watson, J.T., Welch, H., Beltran-Perez, O., Chaffron, S., Greenberg, D.S., Kühn, B., Kiko, R., Lo, M., Lopes, R.M., Möller, K.O., Michael, W., Pala, A., Romagnan, J.B., Schuchert, P., Seydi, V., Villasante, S., Malde, K., Irisson, J.-O., 2023. Machine learning in marine ecology: an overview of techniques and applications. ICES J. Mar. Sci. 80 (7), 1829–1853. https://doi.org/10.1093/icesjms/fsad100.
Rufino, M.M., Mendo, T., Samarão, J., Gaspar, M.B., 2023. Estimating fishing effort in small-scale fisheries using high-resolution spatio-temporal tracking data (an implementation framework illustrated with case studies from Portugal). Ecol. Indic. 154, 110628. https://doi.org/10.1016/j.ecolind.2023.110628.
Russo, T., Pulcinella, J., Parisi, A., Martinelli, M., Belardinelli, A., Santojanni, A., Cataudella, S., Colella, S., Anderlini, L., 2015. Modelling the strategy of mid-water trawlers targeting small pelagic fish in the Adriatic Sea and its drivers. Ecol. Model. 300, 102–113. https://doi.org/10.1016/j.ecolmodel.2014.12.001.
Salas, S., Gaertner, D., 2004. The behavioural dynamics of fishers: management implications. Fish Fish. 5 (2), 153–167. https://doi.org/10.1111/j.1467-2979.2004.00146.x.
Samarão, J., Moreno, A., Gaspar, M.B., Rufino, M.M., 2025. Improving machine learning predictions to estimate fishing effort using vessel's tracking data. Eco. Inform. 85, 102953. https://doi.org/10.1016/j.ecoinf.2024.102953.
Samsun, O., Kalaycı, F., Samsun, N., Bilgin, S., 2006. Karadeniz'de Orta Su Trolü İle Avlanan Pelajik Balıkların Bazı Biyolojik Özellikleri ve Avcılık Verilerinin İncelenmesi. Ege J. Fish. Aquat. Sci. 23 (3), 487–493.
Shockley, Kevin, Santana, Maria-Vee, Fowler, Carol A., 2003. Mutual interpersonal postural constraints are involved in cooperative conversation. J. Exp. Psychol. Hum. Percept. Perform. 29 (2), 326–332. https://doi.org/10.1037/0096-1523.29.2.326.
Spearman, C., 1904. The proof and measurement of association between two things. Am. J. Psychol. 15 (1), 72–101. https://doi.org/10.2307/1412159.
Strandburg-Peshkin, A., Farine, D.R., Couzin, I.D., Crofoot, M.C., 2015. Shared decision-making drives collective movement in wild baboons. Science 348 (6241), 1358–1361. https://doi.org/10.1126/science.aaa5099.
Taconet, M., Kroodsma, D., Fernandes, J.A., 2019. Global Atlas of AIS-based Fishing Activity - Challenges and Opportunities. FAO, Rome (also available at www.fao.org/3/ca7012en/ca7012en.pdf.
Takens, F., 1981. Detecting strange attractors in turbulence. In: Springer Lecture Notes in Mathematics, 898, pp. 366–381. https://doi.org/10.1007/BFb0091924.
Theiler, J., 1986. Spurious dimension from correlation algorithms applied to limited time-series data. Phys. Rev. A 34 (3), 2427–2432. https://doi.org/10.1103/PhysRevA.34.2427.
Tu, E., Zhang, G., Rachmawati, L., Rajabally, E., Huang, G.B., 2018. Exploiting AIS data for intelligent maritime navigation: a comprehensive survey from data to methodology. IEEE Trans Intell Transp Syst 19 (5), 1559–1582. https://doi.org/10.1109/TITS.2017.2724551.
Vermard, Y., Rivot, E., Mahévas, S., Marchal, P., Gascuel, D., 2010. Identifying fishing trip behaviour and estimating fishing effort from VMS data using Bayesian hidden Markov models. Ecol. Model. 221, 1757–1769. https://doi.org/10.1016/j.ecolmodel.2010.04.005.
Vespe, M., Gibin, M., Alessandrini, A., Natale, F., Mazzarella, F., Osio, G.C., 2016. Mapping EU fishing activities using ship tracking data. J. Maps 12 (sup1), 520–525. https://doi.org/10.1080/17445647.2016.1195299.
Wasserman, S., Faust, K., 1994. Social Network Analysis: Methods and Applications. Cambridge University Press. https://doi.org/10.1017/CBO9780511815478.
Watson, J.T., Haynie, A.C., 2016. Using vessel monitoring system data to identify and characterize trips made by fishing vessels in the United States North Pacific. PloS One 11, e0165173. https://doi.org/10.1371/journal.pone.0165173.
Webber Jr., C.L., Zbilut, J.P., 1994. Dynamical assessment of physiological systems and states using recurrence plot strategies. J. Appl. Physiol. 76 (2), 965–973. https://doi.org/10.1152/jappl.1994.76.2.965.
Wilson, E.B., 1927. Probable inference, the law of succession, and statistical inference. J. Am. Stat. Assoc. 22 (158), 209–212. https://doi.org/10.2307/2276774.
Yang, Y., Liu, Y., Li, G., Zhang, Z., Liu, Y., 2024. Harnessing the power of machine learning for AIS data-driven maritime research: a comprehensive review. Transport. Res. E 183, 103426. https://doi.org/10.1016/j.tre.2024.103426.
Yildiz, T., Cömert, N., Ferrà, C., Şaşmaz, U., Galdelli, A., Tassetti, A.N., 2025. Environmental and behavioral drivers of automatic identification system gaps of Turkish trawlers in the Black Sea. Front. Mar. Sci. 12, 1647930. https://doi.org/10.3389/fmars.2025.1647930.
Zeileis, A., Grothendieck, G., 2005. Zoo: S3 infrastructure for regular and irregular time series. J. Stat. Softw. 14 (6), 1–27. https://doi.org/10.18637/jss.v014.i06.
Zengin, M., Düzgüneş, E., Dinçer, A.C., Mutlu, C., Bahar, M., Tabak, İ., 2003. Karadeniz'de Ortasu Trolünün Kullanım Olanakları ve Av Verimliliğinin Araştırılması. In: TAGEM/HAYSUD/1998/17/03/007, Nolu Proje Raporu, T.K.İ.B. Su Ürünleri Araştırma Enstitüsü, Trabzon.
Zhang, C.L., Chen, Y., Xu, B.D., Xue, Y., Ren, Y.P., 2022. The dynamics of the fishing fleet in China seas: a glimpse through AIS monitoring. Sci. Total Environ. 819, 153150. https://doi.org/10.1016/j.scitotenv.2022.153150.